

Compact groups from the Millennium Simulations: I. Their Nature and the completeness of the Hickson sample

Eugenia Díaz-Giménez^{1,2} & Gary A. Mamon^{3,4}

¹ Instituto de Astronomía Teórica y Experimental, IATE, Observatorio Astronómico, Laprida 854, Córdoba, Argentina

² Consejo de Investigaciones Científicas y Técnicas de la República Argentina (CONICET)

³ Institut d’Astrophysique de Paris (UMR 7095: CNRS & Univ. Pierre & Marie Curie) 98 bis Bd. Arago, F-75014 Paris, France

⁴ Astrophysics & BIPAC, Department of Physics, University of Oxford, Oxford OX1 3RH, UK

19 August 2019

ABSTRACT

We identify compact groups of galaxies (CGs) within mock galaxy catalogues from the Millennium Simulation at $z=0$ with the semi-analytic models (SAMs) of galaxy formation of Bower et al., Croton et al. and De Lucia & Blaizot. CGs are identified using the same 2D criteria as those visually applied by Hickson (1982) to his CGs (HCGs), but with a brightest galaxy magnitude limit, and we also add the important effect of observers blending close projected pairs. Half of the mock CGs identified in projection contain at least 4 accordant velocities ($mvCGs$), versus 70% for HCGs. In comparison to $mvCGs$, the HCGs are only 8% complete at distances $< 9000 \text{ km s}^{-1}$, missing the CGs with small angular sizes, a strongly dominant galaxy, and (for the second SAM) the $mvCGs$ that are fainter and those with lower surface brightness. 10% of the mock $mvCGs$ are identical to the parent virialized group, meaning that they are isolated, while the remainder are embedded in their parent virialized groups. We explore different ways to determine the fraction of physically dense groups given the data from the simulations. Binding energy criteria turn out to be inapplicable given the segregation between galaxies and dark matter particles. We rely instead on the combination of the three-dimensional length of the CGs (maximum real space galaxy separation) and their elongation along the line-of-sight (ratio of maximum line-of-sight to maximum projected separations), restricting ourselves in both cases to smallest quartets within the CGs. We find that between 64% and 80% (depending on the SAM) of the $mvCGs$ have 3D lengths shorter than $200 h^{-1} \text{ kpc}$, between 71% and 80% have line-of-sight elongations less than 2, while between 59% and 76% have either 3D lengths shorter than $100 h^{-1} \text{ kpc}$ or both lengths shorter than $200 h^{-1} \text{ kpc}$ and elongations smaller than 2. Therefore, chance alignments (CAs) of galaxies concern at most 40% of the $mvCGs$. These CAs are mostly produced from larger host groups, but a few have galaxies extending a few Mpc beyond the host group. The $mvCGs$ built with the Hickson selection (respectively without the close projected pair blending criterion) have 10% higher (lower) fractions of physically dense systems.

Key words: galaxies: clusters: general – methods: data analysis

1 INTRODUCTION

Compact Groups (CGs) are small, relatively isolated systems of typically four or five luminous galaxies in close proximity to one another. The first example of a CG was found by Stephan (1877). Several catalogues of CGs are now available: Rose (1977) and Hickson (1982) visually identified CGs on POSS I photographic plates. After the Hickson compact group (HCG) catalogue, several CG catalogues have been automatically extracted from galaxy catalogues, themselves automatically extracted from

photographic plates: from the COSMOS/UKST Southern Galaxy Catalog (Prandoni, Iovino, & MacGillivray 1994; Iovino 2002), from the DPOSS catalogue (Iovino et al. 2003; de Carvalho et al. 2005) or CCD frames from the Sloan Digital Sky Survey (SDSS) photometric catalogue (Lee et al. 2004). CG catalogues have also been extracted from galaxy catalogues in redshift space: from the CfA2 (Barton et al. 1996), Las Campanas (Allam & Tucker 2000), and SDSS (Deng et al. 2007; McConnachie et al. 2009) surveys, as well as from the 3D UZC Galaxy Catalog (Focardi & Kelm

2002). CGs are so compact that the median projected galaxy separation in HCGs is only $39 h^{-1}$ kpc (Hickson et al. 1992).

HCGs have been studied in detail, in particular their internal structures, shapes, morphologies, luminosities, and environments (Hickson 1982; Hickson et al. 1984; Mamon 1986; Hickson et al. 1988; Hickson & Rood 1988; Mendes de Oliveira & Hickson 1991; Zepf 1993; Moles et al. 1994; Prandoni et al. 1994; Kelm & Focardi 2004; Tovmassian et al. 2006). To summarise, these studies indicate that CG galaxies have star formation properties, colours and morphological mixes that lie in between binary galaxies and isolated ones.

The nature of the CGs has been a puzzling matter for quite some time. How can a few bright galaxies coexist within less than 100 kpc, given that galaxies are expected to merge fast in such systems (Carnevali, Cavaliere, & Santangelo 1981; Barnes 1985; Mamon 1987; Bode, Cohn, & Lugger 1993)? There are three schools of thought on this matter. One view is that compact groups are recently formed dense systems that are about to coalesce into a single galaxy (Hickson & Rood 1988). The galaxies lost in the merger may be replenished by galaxies in the loose group environment (Diaferio, Geller, & Ramella 1994), and the predicted rate of formation of CGs appears to be sufficient to explain the observed frequency of HCGs (Mamon 2000). The second view states that CGs may be transient unbound cores of looser groups (Rose 1977; Ramella et al. 1994; Tovmassian et al. 2001). And the third scenario places CGs as chance alignments of galaxies along the line of sight within larger loose groups (Rose 1977 for CGs elongated in projection; Mamon 1986 and Walke & Mamon 1989 in general), clusters (Walke & Mamon 1989) and cosmological filaments (Hernquist, Katz, & Weinberg 1995). In this scenario, the numerous signs of interaction and star formation is explained by the frequent occurrence of binaries and triplets in the chance alignments (Mamon 1992).

If CGs are physically dense, their dynamical times should be short (1% of the age of the Universe), and the hot intra-group gas should trace a smooth gravitational potential. The launch of X-ray observatories with good sensitivity in the soft X-ray band (ROSAT, ASCA, Chandra and XMM-Newton) has led to the detection of hot X-ray emitting gas from many CGs. Since the X-ray emissivity scales as the square of the gas density, X-ray emission is less prone to projection effects than optical surveys (but see Ostriker, Lubin, & Hernquist 1995). However, although 22 HCGs were detected out of 32 pointed observations (Ponman et al. 1996), it is not clear what the global fraction of detections would be on the full sample of HCGs (69 [92] groups with at least 4 [3] accordant velocities, according to Hickson et al. 1992). Moreover, some of the detected groups appear clumpy (e.g. HCG 16 according to Dos Santos & Mamon 1999), which strongly suggests their unvirialized state.

The distinction between compact groups that are dense in 3D, or chance alignments within loose groups or longer filaments is difficult, because redshift space distortion introduces uncertainties in the computation of the line of sight coordinate which might result in misidentified compact configurations. For a group with line of sight velocity dispersion σ_v , the redshift distortion will amount to a spread

of $\delta r_z = \sigma_v/H_0$ in the line of sight coordinate. Assuming that the square velocity dispersion is half the square circular velocity at the virial radius, $\sigma_v^2 = (1/2)GM(r_v)/r_v$ (appropriate for an $\rho \propto 1/r^2$ density profile), one finds $\delta r_z/r_v = (1/2)\sqrt{100} = 5$ if the virial radius is defined where the mean density at that radius is 100 times the critical density of the Universe. So redshift space distortions prevent measuring distances within virial systems (see also the Introduction of Walke & Mamon 1989).

Nevertheless, there is one CG meeting the HCG criteria discovered by one of us (Mamon 1989) that is so close (within the Virgo cluster) that surface brightness fluctuation distance measurements by Mei et al. (2007) are able to settle the issue of its nature: Mamon (2008) concludes that this CG is a chance alignment of galaxies along the line of sight, at least 440 kpc and most probably 2 Mpc long.

In summary, even though many efforts have been devoted to look for an explanation about the nature of CGs, the debate is still wide open.

The advent of increasingly realistic cosmological simulations now allow one to distinguish whether CGs are truly dense in 3D, or caused by chance alignments within looser groups, filamentary structures, or the general field. In an early pioneering attempt, Hernquist, Katz, & Weinberg (1995), who identified galaxies as dense knots of cold gas in their N -body + hydrodynamical simulation, and searched for CGs in redshift space in many viewing directions. They found four CGs with at least 4 accordant velocities, all of which were longer than $2 h^{-1}$ Mpc along the line of sight (one was as long as $4 h^{-1}$ Mpc), and yet presented accordant velocities, despite the (Hubble law) stretching of velocities caused by their elongation along the line of sight. The analysis of Hernquist et al. suffers from several drawbacks (according to present-day standards for cosmological simulations): the simulation box was small ($44 h^{-1}$ Mpc wide), the mass resolution was poor (their simulation had 32^3 dark matter particles and 32^3 gas particles, and their galaxies were identified with as few as 8 gas particles), and the spatial resolution was poor (the dark matter particles had a softening length of $10 h^{-1}$ kpc). Furthermore, the identification of galaxies with knots of dense gas was not optimal, especially that feedback from supernovae and active galactic nuclei were not incorporated.

In this work, we quantify the fraction of CGs that can be considered as physically dense entities in samples of automatically identified CGs, based upon more realistic cosmological N body simulations. At present, one can build realistic CGs in two ways: 1) from dissipationless cosmological simulations on top of which galaxies are painted using fairly complex semi-analytical galaxy formation/evolution models; 2) from hydrodynamical codes that resolve galaxies. We have chosen the first approach and use for this purpose the largest cosmological N body simulation ever performed (in 2006, when the present study began), the Millennium Run (Springel et al. 2005), on which galaxies were identified in three ways, using three different state-of-the-art semi-analytic models (SAMs) of galaxy formation (Bower et al. 2006; Croton et al. 2006; De Lucia & Blaizot 2007).

These three galaxy samples provide an opportunity to test both, projection effects and the real nature of systems identified using standard algorithms like that proposed by Hickson (1982). The CGs are identified in mock redshift-

space catalogues constructed from the real-space galaxy sample derived with the semi-analytical model, from the Millennium Run.

In comparison with the analysis of Hernquist et al., our study is based upon a simulation in a box whose volume is over 1 million times greater, with 30 thousand times as many particles, 25 times finer mass resolution and a softening scale 4 times smaller. However, the simulation we use does not contain gas particles, so the galaxy parameters are highly dependent on the physics of galaxy formation and evolution of the three SAMs that we analyse.

We focus here on the HCG catalogue, which is by far the best studied sample of Compact Groups.

The layout of this paper is as follows. In Section 2, we present the different steps for the construction of the mock CG catalogue and Sect. 3 describes how the resulting CGs are classified. The conclusions are summarised and discussed in Section 4. Once our analysis was well advanced, we learnt about the work of McConnachie et al. (2008), who performed a similar analysis of the properties of Hickson-like CGs from the De Lucia & Blaizot (2007) galaxy catalogue, and found that 70% of the mock CGs selected in projection were caused by chance alignments of galaxies. We highlight in Sect. 4.2 the similarities and several important differences between our two studies.

2 CONSTRUCTION AND CLASSIFICATION OF THE COMPACT GROUP SAMPLE

2.1 Observed compact group sample

We use the HCG catalogue of compact groups, with photometry measured by Hickson, Kindl, & Auman (1989) in the B and (presumably Johnson) R bands. Hickson (1982) found 100 HCGs, and Hickson et al. (1992), who measured the redshifts for virtually all galaxies, built a velocity sample of $vHCGs$ by eliminating galaxies lying at more than 1000 km s^{-1} from the group's median velocity. In this manner, they obtained 92 HCGs with at least 3 accordant velocities and 69 HCGs with at least 4 accordant velocities. We extracted the photometry and velocities using Table VII/213/galaxies in Vizier¹ (Ochsenbein, Bauer, & Marcout 2000). This database contains the velocities for all galaxies except 6. We found the redshifts for these 6 galaxies (Table 1) in the NASA/IPAC Extragalactic Database (NED)².

For future comparisons with the SDSS, we choose a Johnson R -band magnitude limit of 17.44 that mimics the SDSS spectroscopic magnitude limit of $r < 17.77$ (see appendix A). We measure the total raw magnitude R_T and the extinction-corrected magnitude R_T^0 using

$$\begin{aligned} R_T &\simeq B_T - (B - R), \\ R_T^0 &\simeq B_T^0 - (B - R) + E_{B-R}, \\ E_{B-R} &= (B_T - B_T^0) \left(1 - \frac{A_R/A_V}{A_B/A_V} \right), \end{aligned}$$

where B_T , B_T^0 and $B - R$ are the raw total blue magnitude,

Table 1. Additional HCG galaxy redshifts found in NED

Galaxy	v (km s^{-1})	$\epsilon(v)$ (km s^{-1})	Reference
18b	4105	25	Falco et al. (1999)
19c	4253	23	de Carvalho et al. (1997)
19d	20443	26	de Carvalho et al. (1997)
51g	7532	41	de Vaucouleurs et al. (1991)
57h	9240	105	Hickson (1993); Barton et al. (1998)
100d	5590	32	Hickson (1993)

Notes: The radial heliocentric velocities and their errors are given in columns 2 and 3, respectively. For HCG57h, the velocity is from the first reference, while the error is from the second.

extinction-corrected total blue magnitude and isophotal $B - R$ colour, all given in VizierR.

We first note that only 83 HCGs out of the original 99³ have at least 4 galaxies whose extinction-corrected R -band magnitudes are within 3 mag from the brightest one.⁴ Six of the HCGs do not satisfy the HCG isolation criterion (Sulentic 1997) and these were also omitted from our sample. On the other hand, we re-inserted into our sample HCG 31, which has additional members (Sulentic 1987), among which two additional members within 3 magnitudes from the brightest member: galaxies G and Q, for which we adopt the R -band photometry of Rubin et al. (1990), while the radial velocities are taken from Mendes de Oliveira et al. (2006), and convert to R_T^0 using the median difference for other galaxies: $R_T^0 = R - 0.38$.

We are left with 72 HCGs whose brightest magnitude satisfies $R_b < 17.44 - 3 = 14.44$, thus ensuring completeness out to $R = 17.44$. We call this the $pHCG$ sample (for HCGs defined in projected space).

Only 52 among the 72 $pHCGs$ have at least 4 galaxies within 1000 km s^{-1} from the median group velocity (hereafter the $vHCG$ sample, for velocity-selected HCG).

2.2 Basic scheme for mock compact group samples

Our mock catalogues of CGs are built in several steps, in which we:

- (i) simulate the gravitational evolution of a large piece of the Universe, represented by collisionless (dark matter) particles;
- (ii) attach galaxies to the simulation with a semi-analytical galaxy formation model
- (iii) convert to a mock galaxy catalogue in redshift space;
- (iv) convert to a mock 2D CG catalogue (hereafter $mpCG$ for mock CG in projection), by applying the HCG selection criteria;
- (v) convert the $mpCG$ catalogue to a velocity-filtered

³ We have omitted group HCG 54, which is the HCG with the smallest projected radius, as it appears to be either a group of H II regions in a single galaxy (Arhipova et al. 1981) or the end result of the merger of two disk galaxies (Verdes-Montenegro et al. 2002).

⁴ This is also clear in the B_T and B_T^0 magnitudes given in Hickson et al. 1989, although this was not discussed by these authors, but was also noted by Sulentic (1997).

¹ <http://webviz.u-strasbg.fr/viz-bin/VizieR>

² <http://nedwww.ipac.caltech.edu>

mock CG catalogue (hereafter, *mvCG* for mock velocity-filtered CG), by removing galaxies with discordant redshifts;

(vi) convert the *mvCG* catalogue to a mock velocity-filtered HCG catalogue (hereafter, *mvHCG* for mock velocity-accordant Hickson Compact Group), by randomly selecting groups according to the completeness of the HCG as a function of group surface brightness, brightest galaxy magnitude and its contribution to the total group luminosity.

The last step is motivated by the strong incompleteness of the HCG catalogue in surface magnitude and galaxy magnitude (see Sect. 2.7, below).

A list of the different acronyms used to refer to the different samples is provided in Table 2.

2.3 Dark matter particle simulation

We use the Millennium Simulation, which is a cosmological Tree-Particle-Mesh (TPM, Xu 1995) N -body simulation (Springel et al. 2005), which evolves 10 billion (2160^3) dark matter particles in a $500 h^{-1}$ Mpc periodic box, using a co-moving softening length of $5 h^{-1}$ kpc.⁵ The cosmological parameters of this simulation correspond to a flat cosmological model with a non-vanishing cosmological constant (Λ CDM): $\Omega_m = 0.25$, $\Omega_\Lambda = 0.75$, $\sigma_8 = 0.9$ and $h = 0.73$. The simulation was started at $z = 127$, with the particles initially positioned by displacing particles initially in a glass-like distribution according to the Λ CDM primordial density fluctuation power spectrum. The 10^9 particles of mass $8.6 \times 10^8 h^{-1} M_\odot$ are then advanced with the TPM code, using 11 000 internal time-steps, on a 512-processor supercomputer. The positions and velocities of the 10 billion particles were saved at 64 epochs (leading to nearly 20 TB of data).

2.4 Modelling galaxies

We consider the $z = 0$ outputs from three different SAMs of galaxy formation by Bower et al. (2006), Croton et al. (2006), and De Lucia & Blaizot (2007), (B06, C06 and DLB, respectively), where each model was applied in turn to the outputs of the Millennium Simulation described above. Note that, while the B06 and C06 models were developed independently, the DLB model is essentially the same as the C06 model, except that the merger rate is reduced by a factor 2, the magnitudes are derived using spectral synthesis models based upon a different initial mass function (Chabrier 2003 instead of Salpeter 1955) with fewer low mass stars, and the treatment of radiative transfer to dust is much more refined.

The three SAMs produce galaxy positions, velocities, as well as absolute magnitudes (in five or more optical and near-infrared wavebands, all including Johnson R), as well as other quantities. To summarise, the branches of the halo merger tree (produced by the Millennium Simulation) are followed forward in time, and the following astrophysical processes are applied: gas infall and cooling, early reheating of the intergalactic medium by photoionization, star

formation, black hole growth, AGN and supernova feedback, galaxy mergers, spectro-photometric evolution, etc. The model parameters have been adjusted to produce a good match to the observed properties of local galaxies. In these SAMs, AGN feedback is responsible for the absence of cooling flows in rich clusters, for the cut-off at the bright end of the galaxy luminosity function and for the number density properties of the most massive galaxies at all redshifts. Also, the early reheating of the IGM by photoionization is responsible for suppressing gas cooling in halos below a circular velocity that is independent of redshift (or nearly so). The 3 SAMs produce $z = 0$ galaxy luminosity functions that are in good agreement with observations in both the b_J and K wavebands,⁶ with an excess of galaxies at very bright luminosities for all 3 models and a slight excess at faint luminosities for the C06 and DLB models. Moreover, the B06 SAM provides several other observational predictions: the b_J and K galaxy luminosity functions at higher redshifts, the global history of star formation, and the local black hole mass vs. bulge mass relation.

All three SAMs produce around 10 million galaxies at $z = 0$. The galaxy samples appear to be complete at least to $M_R - 5 \log h < -17.4$ with stellar masses $M_* > 10^9 h^{-1} M_\odot$ (C06) or $M_* > 3 \times 10^8 h^{-1} M_\odot$ (B06, DLB).

Each of the three SAMs has its strengths and weaknesses. The B06 model computes galaxy mergers by inferring the positions of galaxies in their halo through typical values of their energies and angular momentum in units dimensioned to the virial scales of the halos. In contrast, the C06 and DLB models have the advantage of estimating the merger rates directly from the positions of subhaloes in the dark matter simulation. They both use the same analytical formula for the orbital decay time by dynamical friction once the subhalo masses fall below their resolution limit, where the DLB time is twice the C06 time, which itself matches almost perfectly the decay time that Jiang et al. (2008) calibrated on high-resolution cosmological hydrodynamical simulations. Unfortunately, C06 do not provide the galaxy merger trees, so it is difficult to derive the history of star formation of a given galaxy. Also, while B06 find a Red Sequence with increasing red colours for increasingly higher stellar masses, the C06 catalogue shows a colour-luminosity relation for the Red Sequence galaxies that flattens at high luminosity, contrary to observations, and a similar effect is seen in the DLB galaxy output (as shown by Bertone et al. 2007). Still, the B06 colours are too blue and fit somewhat less well the SDSS colour distribution than do the DLB colours (Mateus et al. 2008). The SAM of Cattaneo et al. (2006) reproduces better the colours of galaxies, but its output is not public and the galaxy positions are determined stochastically (like B06) rather than by following the dark matter subhaloes (like C06 and DLB). The DLB catalogue produces galaxies whose present-day small-scale segregation of recently formed stellar mass is too large, while that of B06 matches well that observed with the SDSS (Mateus et al.). This is surprising given that the B06 model treats galaxy mergers using stochastic positions rather than the positions of the subhaloes with which the galaxies are associated (see

⁵ The Millennium Simulation, run by the Virgo Consortium, is publicly available at <http://www.mpa-garching.mpg.de/millennium>

⁶ The $z = 0$ luminosity function of the De Lucia & Blaizot (2007) model is given by Bertone et al. (2007).

Table 2. List of acronyms used throughout this work

CG	general compact groups
HCG	Hickson compact groups
<i>pHCG</i>	HCGs that strictly meet the Hickson (1982) criteria $+R_b \leq 14.44$
<i>vHCG</i>	velocity accordant <i>pHCGs</i>
<i>pmpCG</i>	particle mock projected compact groups, which strictly meet the Hickson (1982) criteria $+R_b \leq 14.44$
<i>mpCG</i>	observable mock projected compact groups (same as <i>pmpCGs</i> , but accounting for galaxy confusion)
<i>pmvCG</i>	particle mock velocity accordant compact groups
<i>mvCG</i>	observable mock velocity accordant compact groups (same as <i>pmvCGs</i> , but accounting for galaxy confusion)
<i>mvHCG</i>	observable mock velocity accordant compact groups with Hickson’s biases
CA	chance alignment of galaxies
CALG	chance alignment of galaxies within looser groups
CAF	chance alignment of galaxies within filaments
<i>PG3D</i>	Parent groups identified in real space

above). However, the DLB model predicts a little better than B06 the analogous segregation for intermediate age (0.2–0.5 Gyr) stellar mass (Mateus et al.). But the present-day galaxy merger rate of DLB appears too low, while that of B06 matches well the observations of the frequency of galaxy pairs (Mateus 2008).

In summary, it is very difficult to decide which of the three SAMs is most appropriate for our study of CGs, and we therefore decided to analyse the outputs of all three of them. We will find and illustrate several important differences in the properties of mock CGs predicted from these three models.

2.5 Mock galaxy catalogues

Using the snapshots at $z = 0$, we construct mock catalogues in redshift space. For the three SAMs, we obtain redshifts by adding the Hubble flow to the peculiar velocities projected in the line of sight direction. We compute the observer-frame galaxy apparent magnitudes from the rest-frame absolute magnitudes provided by the semi-analytical model. These apparent magnitudes are converted to the observer frame using tabulated $k + e$ corrections (Poggianti 1997).

Our mock catalogue is constructed by viewing the full volume of the simulation box from one of its 8 vertexes ($z_{\max} \sim 0.17$, $\pi/2 \text{ sr} = 5156 \text{ deg}^2$) We set an apparent magnitude limit $R = 17.44$, equal to the limit we set on the HCG groups to match the SDSS spectroscopic catalogue for later comparisons (see Sect. 2.1).

In order to increase the statistical significance of our results, we considered eight observers situated at the eight vertexes of the simulation box, and all the identification procedures were performed on these eight samples to finally combine the resulting CGs into one larger sample. These eight samples are almost fully statistically independent, since 3/4 of the mock CGs selected in the cone (see Fig. 3) lie within half the box size ($256 h^{-1} \text{ Mpc}$) (see upper right panel of Fig. 2). Table 3 summarises the main properties of the three mock galaxy catalogues seen from one of its vertexes.

The completeness of our magnitude+volume limited mock catalogues might be an important issue that could bias the results. The implications on the results of using magnitude+volume limited samples will be carefully tested in Sect. 2.8.

We identify regular groups of galaxies in the simulation box by applying a Friends-of-Friends (FoF) algorithm in real

Table 3. Mock galaxy catalogues ($R < 17.44$)

Mock	#	z_{med}	\bar{n}_{90} ($h^3 \text{ Mpc}^{-3}$)
Bower et al. (2006)	556 224	0.0998	0.062
Croton et al. (2006)	446 153	0.0969	0.059
De Lucia & Blaizot (2007)	1 034 619	0.1114	0.089

Notes: #: number of galaxies seen from a single vertex of the simulation box, z_{med} : median redshift, \bar{n}_{90} : space number density within $90 h^{-1} \text{ Mpc}$, defined in equation (1).

space (Davis et al. 1985) to the galaxies. We adopt a linking length of $l = 0.17 n^{-1/3}$, where n is the mean space density of galaxies. The factor 0.17 roughly corresponds to an overdensity of 100 relative to the critical density of the Universe, roughly the minimum overdensity (hence maximum radius) where cosmological structures are in dynamical equilibrium (Bryan & Norman 1998, but recent work by Cuesta et al. 2008 shows that on the mass scales of groups, the radius of equilibrium is roughly 30% greater). We denote these groups the *PG3Ds* for *Parent groups selected in real space*, and will later check if the mock CGs extend beyond these *PG3Ds*.

2.6 Mock compact groups selected in projected space

In this work, we use an automated *mpCG* search algorithm very similar to that described by Hickson (1982), applied to the three mock galaxy catalogues. The algorithm defines as *mpCGs* those systems that satisfy the following conditions:

- (i) $4 \leq N \leq 10$ (population)
- (ii) $\mu_R < 26 \text{ mag arcsec}^{-2}$ (compactness)
- (iii) $\theta_N > 3 \theta_G$ (isolation)
- (iv) $R_{\text{brightest}} \leq 14.44$ (flux limit)

where

- N is the total number of galaxies whose R -band magnitude satisfies $R < R_{\text{brightest}} + 3$, where $R_{\text{brightest}}$ is the magnitude of the brightest galaxy;
- μ_R is the mean R -band surface magnitude, averaged over the smallest circle circumscribing the galaxy centres.
- θ_G is the angular diameter of this smallest circumscribed circle;
- θ_N is the angular diameter of the largest concentric circle that contains no other galaxies within this magnitude range or brighter;

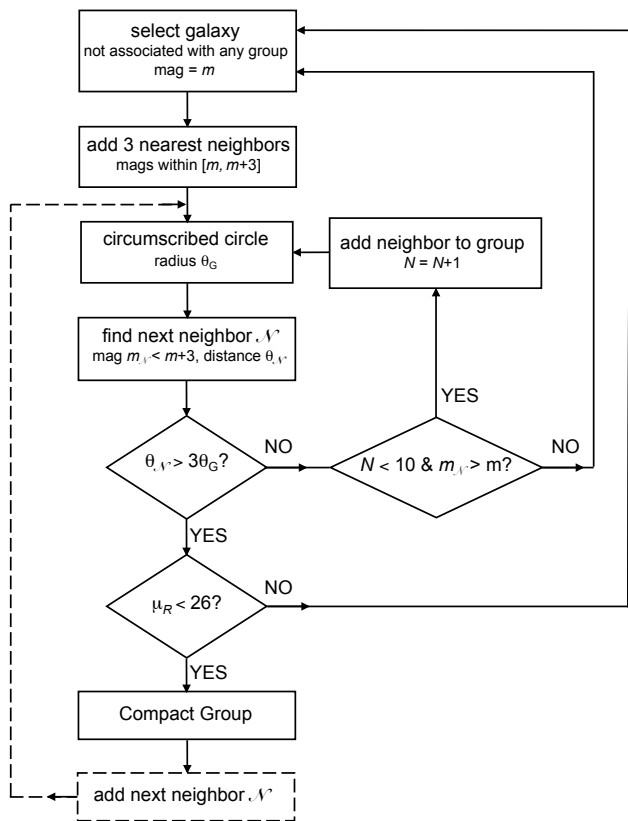


Figure 1. Flowchart of the selection of projected compact groups. All magnitudes must be brighter than our chosen global magnitude limit. The dashed portion allows for compact groups containing isolated compact subgroups.

Note that the fourth criterion (which implies $R_{\text{faintest}} \leq 17.44$) was not considered by Hickson (1982). This restriction is fundamental for avoiding selection biases, as will be demonstrated in Sect. 2.8.

The main steps of this algorithm are summarised in the flowchart of Figure 1.

Now, some CGs meeting Hickson’s criteria might be embedded within larger CGs that also meet Hickson’s criteria (with larger isolation annuli). For such groups, we thus have two choices for our CG selection algorithm: select the smaller (sub-)group (solid portion only in the flowchart of Figure 1) or the larger group (with the dashed portion of the flowchart of Figure 1). The percentages of CGs containing smaller CGs are 13%, 10% and 6% for B06, C06 and DLB models, respectively. The HCG sample was selected according to the larger group (P. Hickson, private communication). However of the 100 groups in the original HCG sample, only one has a definite subgroup (HCG 17). Therefore, it is not clear that P. Hickson always followed the larger group algorithm. In what follows, we adopt the larger group algorithm (i.e. including dashed portion of the flowchart of Figure 1). However, our results turn out to depend little on the choice among these two algorithms.

To accelerate this algorithm, we have used the subroutines of the HEALPix⁷ package to find neighbours, and the STRIPACK⁸ subroutines to compute the centres and radii of the minimum circles. Given that our mock catalogues have edges (the limits of the cone), we discarded CGs lying near the edges since those groups will be fictitiously isolated. Then, we kept with a safe sample of CGs that lies in the range $\alpha > 5^\circ$ & $\alpha < 85^\circ$, and $\delta > 5^\circ$ & $\delta < 85^\circ$ (solid angle $\Delta\Omega = 1.2693$ sr).

Using this algorithm, we find 7580, 4756 and 15383 mock CGs in the B06, C06 and DLB samples, respectively.

Now, the galaxies in the mock galaxy catalogues are simply point particles. However, when one observes two galaxies that lie so close in projection on the plane of the sky that their isophotes overlap, they risk being blended into a single object. This galaxy confusion can be important for CGs, which by definition often have overlapping isophotes. For example, observed CG catalogues should have fewer very dense groups than mock CG catalogues. We therefore included one extra *observability* criterion: two galaxies are confused and blended if their projected separation is smaller than the sum of their half light radii, in which case we sum their luminosities and adopt the redshift of the most luminous galaxy. For galaxies in the mock catalogues, the half light radii were computed as a function of their absolute magnitude in the R-band, according to Shen et al. (2003, eqs. [14] and [15] therein).

Hereafter (see Table 2), we refer to these observable mock projected compact groups as *mpCGs* and denote the original ones as *pmpCGs* (for *particle-mock-projected compact groups*). The *mpCGs* are built with the Hickson criteria given at the beginning of Sect. 2.6 and thus contain at least 4 galaxies (after the pair-blending procedure). We understand that our pair-blending criterion is simplistic and may be somewhat liberal in defining confused galaxy pairs. In reality, observed CGs should lie in between our *pmpCGs* and our *mpCGs*, but probably much closer to the *mpCGs*. We therefore adopt the observable criterion (hence, the *mpCGs*) in what follows, unless explicitly stated otherwise.

2.7 Mock compact groups after velocity filtering

We then built a sample of *velocity-filtered mock compact groups* on top of the respective *pmpCG* and *mpCG* samples, which we call the *pmvCG* (*particle-mock-velocity-filtered compact group*) and *mvCG* (*mock velocity-filtered compact group*) samples (see Table 2) with the following iterative procedure (see Hickson et al. 1992):

- Compute the median velocity of the group, v_{median} .
- Discard those galaxies with $|v - v_{\text{median}}| > 1000 \text{ km s}^{-1}$.
- If at least n_{min} galaxies remain, iterate until no galaxies are dropped or the group disappears ($n < n_{\text{min}}$),
- Save those CGs that have at least n_{min} galaxies and that satisfy the compactness criterion.

We call n the number of accordant-velocity galaxies in the *mvCG* and adopt $n_{\text{min}} = 4$ as our minimum number of accordant velocities.

⁷ <http://healpix.jpl.nasa.gov/index.shtml>

⁸ http://people.sc.fsu.edu/~burkardt/f_src/stripack/stripack.html

Table 4. Compact group samples

Sample	Type	gals		v filter	N			\bar{n}_{90} ($10^{-5}h^3\text{Mpc}^{-3}$)		
		obs	ext		B06	C06	DLB	B06	C06	DLB
$pHCG$	obs	ext	no		72			1.9		
$vHCG$	obs	ext	yes		52			1.1		
$mpCG$	mock	par	no		7580	4756	15383	49	33	31
$mpCG$	mock	ext	no		3574	3265	4729	18	23	11
$pmvCG$	mock	par	yes		4553	2685	5646	43	29	23
$mvCG$	mock	ext	yes		2073	2095	2825	16	22	10
$mvHCG$	mock	ext	yes		272	223	291	5.1	5.4	2.6

Notes: Col. 1: sample; col. 2: sample type (obs=observed); col. 3: galaxy type (par=particle; ext=extended); col. 4: velocity filter; col(s). 5: number of groups (summed over 8 vertexes for mocks); col(s). 6: space density within $90 h^{-1} \text{Mpc}$ (eq. [1], divided by 8 for the mock samples to take into account the 8 vertexes from which they were selected). Columns with 3 values show the results for the Bower et al. (B06), Croton et al. (C06), and De Lucia & Blaizot (DLB) SAMs, respectively. The limiting surface magnitude of the $mvHCG$ sample is not sharp.

Table 4 shows the number of groups in the observed and mock CG samples. The percentage of $mpCG$ s that survive the velocity-filtering is 58% (B06), 64% (C06), and 60% (DLB), so that our final samples of accordant velocity CGs contain from ~ 2050 to ~ 2800 $mvCG$ s depending on the adopted SAM.

The main properties of the $mvCG$ s identified in the DLB galaxy catalogue are shown in Figure 2 together with the observed distribution of $vHCG$ s (the distribution of the $mvCG$ s obtained with the other two SAMs are similar, except for radial velocity distributions that are more skewed to lower values and considerably more groups in the bin of lowest group surface brightness). Hickson’s visual selection of CGs produced a catalogue that is incomplete at small angular sizes (middle left plot), faint brightest galaxy magnitudes (middle right plot), and in groups with a dominant brightest galaxy (bottom left plot). We will quantify the completeness of the HCG in Sect. 2.9.

2.8 Testing the volume-limited sample

As we shall now see, limiting the depth of our galaxy sample to the simulation box provides a complete list of $mvCG$ candidates. However, our neglect of galaxies further than the box size may prevent distant galaxies from spoiling the isolation of some of the $mvCG$ s. Although the DLB model is available in an observing cone, this is not the case for the other two SAMs, and while we can construct a cone ourselves by placing galaxies of previous time-steps at the position corresponding to their lookback times, we do not have access to the $z > 0$ outputs of the Croton et al. (2006) model to do this, and we wish to consider all three SAMs in parallel.

We therefore use the DLB model to build a mock sample of galaxies within a cone, built of shells constructed from different snapshots corresponding to the epoch of the lookback time at their distance. Here we use the 17 last snapshots, bringing us to a maximum redshift of $z = 0.68$, where the minimum luminosity, $M_R = -24.91$, corresponds to $45 L_*$.

The top panel in Fig. 3 compares the radial velocity distribution of $mpCG$ s extracted from the volume limited

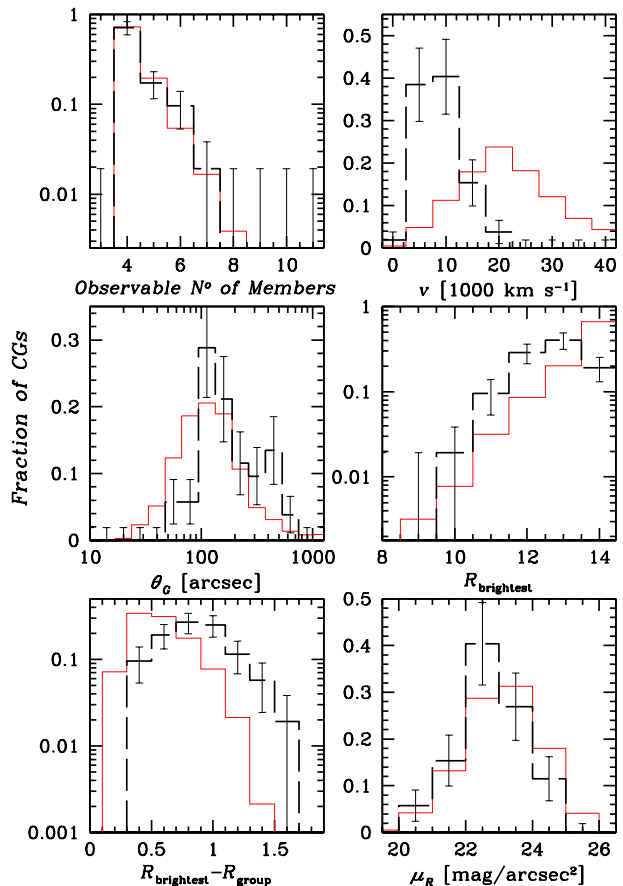


Figure 2. Distributions of properties of the velocity selected CGs: mock $mvCG$ s from the De Lucia & Blaizot (2007) model (thin red histograms) and observed $vHCG$ s (thick black dashed histograms). The properties are the group multiplicities (top left panel), radial velocities (top right panel), angular group diameters (middle left panel), brightest galaxy magnitudes (middle right panel), magnitude differences between the brightest galaxy and the full group (bottom left panel), and group surface brightness (bottom right panel). Error bars correspond to Poisson errors.

mock catalogue described in Sect. 2.5 (solid lines) seen from one of its vertexes with that obtained from groups identified in a magnitude limited mock catalogue or light cone of the same solid angle (dashed lines). It can be clearly seen that the $mpCG$ s obtained from the light cone and from the volume limited catalogue before the $R_{\text{brightest}}$ cut-off (thin lines) are quite different. First, the cone sample is able to detect a large number of $mpCG$ s beyond the limits of the box. On the other hand, fewer $mpCG$ s are identified in the cone sample at small distances (up to 80% of the box size). This lower abundance of $mpCG$ s in the cone sample is the consequence of distant galaxies spoiling the isolation criterion of many mock compact groups. The total number of $mpCG$ s in the cone sample is 4% lower than in the box sample. These differences become more pronounced when the flux limit is applied (thick lines). The number of $mpCG$ s in the cone sample is now 38% lower than that of the box sample. Interestingly, the cone sample of $mvCG$ s (with the bright-

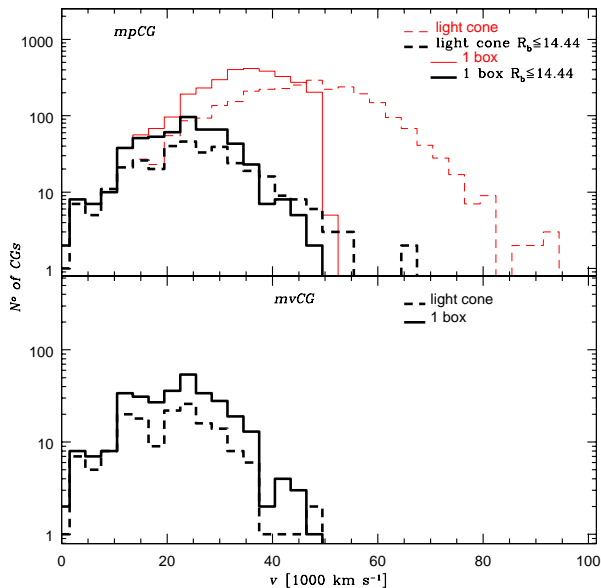


Figure 3. Radial velocity distributions of *mpCGs* (top panel) and *mvCGs* (bottom panel) built from a volume-limited catalogue (solid lines) and from a light cone (dashed lines), both having $R < 17.44$. These catalogues were constructed from the DLB SAM.

est galaxy magnitude limit applied) shows a lack of CGs at all distances in comparison with the analogous box sample. The total number of *mvCGs* in the cone sample is half that of the analogous box sample. This indicates that our *mpCG* box-sample catalogue is only 62% reliable against contamination of the isolation annulus by distant interlopers, while our *mvCG* box-sample catalogue is only 50% reliable.

We can use this comparison of box and cone samples to correct the fraction of *mpCGs* that survive the velocity filter and make it as *mvCGs*: this fraction becomes $0.6 \times 0.5 / 0.62 = 48\% \pm 1$ (where the error is from binomial statistics and neglects the systematic error from the cone to box correction).

2.9 Completeness

2.9.1 Measure of completeness

It is interesting to compare the space density of *mpCGs* and *mvCGs* with those of the observed HCGs, selected in the same way. We estimate for the mock and observed samples the mean total surface density of CGs, as well as the mean space density of CGs within the lowest median distance of all samples, which is a fairly robust measure of density. The adopted distance is 9000 km s^{-1} , which is close to the median of the *vHCG* sample, so the space density is computed as

$$\bar{n}_{90} = \frac{3N(v < 9000 \text{ km s}^{-1})}{90^3 \Delta \Omega} h^3 \text{ Mpc}^{-3}, \quad (1)$$

where v is the median velocity of the group members, while Δ is the solid angle of the sample (in sr).

2.9.2 Projected compact groups

For the *mpCGs*, we obtain 1.8 , 2.3 and $1.1 \times 10^{-4} h^3 \text{ Mpc}^{-3}$ (see Table 4) using the SAMs by B06, C06 and DLB, respectively. In comparison, the HCGs were selected on the POSS I plates, spanning $9.7 \text{ sr} = 32000 \text{ deg}^2$ ($\text{Dec} > -33^\circ$). For the 72 *pHCGs*, the mean density is $\bar{n}_{90} = 1.9 \times 10^{-5} h^3 \text{ Mpc}^{-3}$ (Table 4), i.e. typically 9 times lower than the values obtained from the 3 samples of *mpCGs*.

Now, within a limiting distance of $v = 9000 \text{ km s}^{-1}$, we found (Fig. 3) 17 *mpCGs* in our light cone in comparison with 22 in one of our boxes, again because our box sample misses possible distant interlopers that spoil the CG isolation. This suggests that we would have found 23% fewer *mpCGs*, had we not limited ourselves to the box. We deduce that the observed *pHCG* sample is $(1/9)/(17/22) \sim 14\%$ complete at this limiting distance (which again corresponds to the median distance of the HCG catalogue).

Hickson's inclusion of the Galactic Plane should lead to underestimates of the completeness of roughly 1/3, which is the fraction of his search area ($\delta > -27^\circ$ covered by the POSS I survey) with low galactic latitudes $|b| < 20^\circ$. Therefore, the bulk of the incompleteness of the HCGs lies in the incomplete visual selection at high galactic latitudes.

2.9.3 Velocity-filtered compact groups

We now compare the space density of *mvCGs* with that of the *vHCG* sample. For our mock samples of *mvCGs* with at least 4 accordant velocities, the space densities \bar{n}_{90} are (Table 4) 1.6 , 2.2 and $1.0 \times 10^{-4} h^3 \text{ Mpc}^{-3}$, for B06, C06 and DLB, respectively. For comparison, for the 52 *vHCGs* (defined with at least 4 accordant velocities and with brightest galaxy magnitude brighter than 14.44), the space density is $\bar{n}_{90} = 1.1 \times 10^{-5} h^3 \text{ Mpc}^{-3}$ (Table 4). Therefore, the space density of *mvCGs* selected in the box is typically 15 times that of the observed *vHCG*.

However, within $v < 9000 \text{ km s}^{-1}$, we found 16 *mvCGs* in our light cone versus 20 (20% more) in our box (for a single vertex as observation point). This suggests that we would have found 20% fewer *mvCGs*, had we not limited ourselves to the box (thus allowing for distant galaxies to spoil the isolation of these 20% of the *mvCGs*). Therefore, we deduce that the completeness of the *vHCG* sample is $1/15/(16/20) = 8\%$. Note that we assumed that the contamination of distant galaxies of the isolation criterion of *mpCGs* and *mvCGs* is independent of the SAM, even if we only measured this effect with the DLB model.

The top panels of Fig. 4 show the completeness of the velocity-filtered Hickson sample as a function of radial velocity for the 3 SAMs. The completeness is defined as $C(v) = \bar{n}_{v/H_0}^{vHCG} / \bar{n}_{v/H_0}^{mvCG}$, where $H_0 = 100 \text{ km s}^{-1} \text{ Mpc}^{-1}$. The green arrow shows the limit of our nearby subsample (see Table 4). The next 5 rows of panels show the completeness within the nearby subsamples ($v < 9000 \text{ km s}^{-1}$) $C = \bar{n}_{90}^{vHCG} / \bar{n}_{90}^{mvCG}$, as a function of the other observable properties for the nearby subsample.

For all 3 SAMs, the *vHCG* completeness decreases sharply with distance (top panel), for groups with a dominant brightest galaxy (bottom panel), while the C06 model also predicts a decrease of *vHCG* completeness at fainter magnitude and lower surface brightness, whereas these

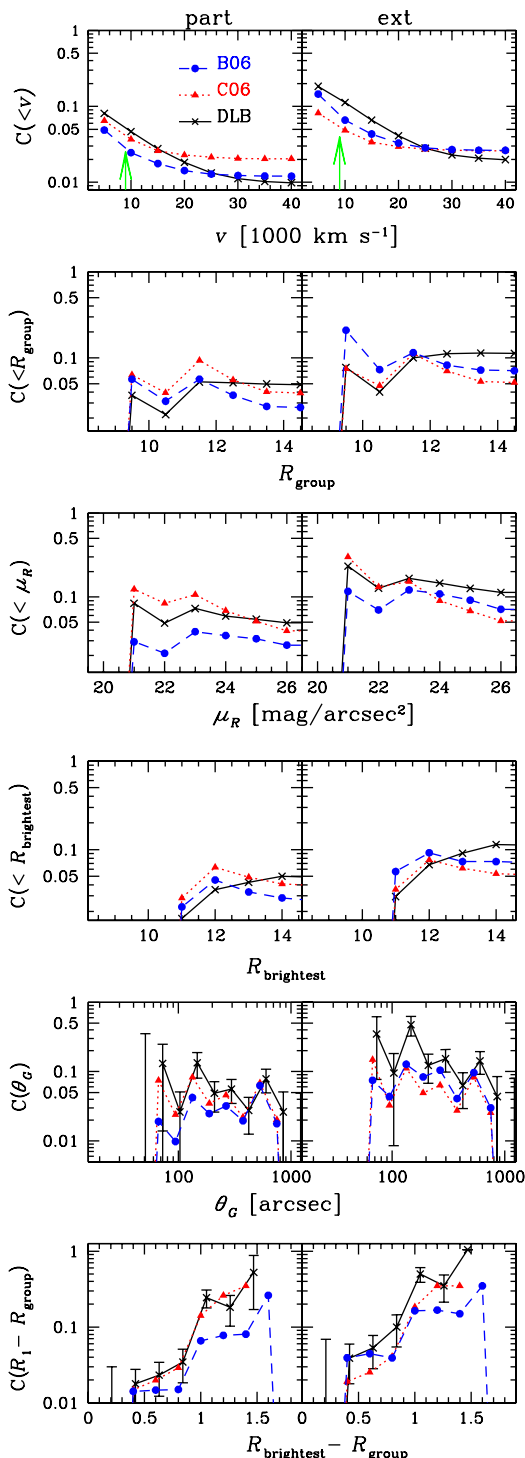


Figure 4. Completeness of the $vHCG$ catalogue relative to the $pmvCG$ (left) and $mvCG$ (right) mock catalogues as a function of distance (top panels) and for groups within $v = 9000 \text{ km s}^{-1}$ (other five rows of panels). From top to bottom the panels represent global cumulative completeness vs. distance, vs. group total magnitude, vs. group surface brightness and vs. brightest group galaxy, and differential completeness vs. angular size and vs. dominance of brightest galaxy. The reference SAMs are Bower et al. (blue circles), Croton et al. (red triangles), and De Lucia & Blaizot (black crosses). Error bars for differential completeness are computed as binomial errors and are shown only for DLB SAM.

trends are weaker in B06 and absent in DLB. Comparing the left and right sets of panels, one sees similar qualitative trends of completeness versus interesting parameter, but with overall completeness relative to the extended-galaxy $mvCGs$ that is roughly double the value of the completeness relative to particle-based $pmvCGs$. Moreover, one can see a slightly faster trend of decreasing completeness with decreasing surface brightness with the C06 model.

2.9.4 Comparison with previous studies

Previous studies have concluded that the $pHCG$ sample is incomplete at low group surface brightness ($24 < \mu_R < 26 \text{ mag arcsec}^{-2}$): Hickson (1982) and Walke & Mamon (1989) (from the lack of low surface brightness groups), and Prandoni, Iovino, & MacGillivray (1994) (from a comparison with their own automatically-selected projected SCG sample of compact groups, built with very similar criteria as Hickson 1982). We also found a large incompleteness at low group surface brightness when comparing the $pHCGs$ with our $mpCG$ samples. However, the sharp drop in the number of compact groups with low surface brightness ($\mu_R > 24$) observed in the $pHCGs$, is also clearly visible in the $mvCGs$ with the DLB model (but less so with the other two SAMs).

The incompleteness in brightest galaxy counts is analogous to the incompleteness in group number counts that Hickson had noticed at $R = 13.0$ and that Prandoni et al. had already noticed at the much brighter limit of $b_J = 13.1$ (from the break in the slope of the number counts away from the Euclidean value of 0.6). Mamon (2000) noted that Fig. 7 of Prandoni et al. indicates that the $pHCG$ catalogue is incomplete by a factor 3 at bright magnitudes, relative to the SCG catalogue, while this incompleteness gets worse at increasingly fainter magnitudes. A closer look at their Fig. 7 reveals that the number of groups brighter than $b_J = 13$ is roughly 30 for the HCG and 2.5 for the Euclidean extrapolation of the SCG group counts to this relatively bright magnitude. Given that the solid angle of the HCG (32000 deg^2) is 25 times that of the SCG (1300 deg^2), the completeness of the HCG relative to the SCG is $30/2.5/25 = 0.48$, with total surface densities of $30/32000 = 0.9 \times 10^{-3} \text{ deg}^{-2}$ and $2.5/1300 = 1.9 \times 10^{-3} \text{ deg}^{-2}$ for the $pHCG$ and SCG, respectively.

This strong incompleteness at faint magnitudes is also evident for $vHCGs$, as seen in the middle right panel of our Fig. 2, which suggests (by matching the magnitude counts at intermediate magnitudes) that the HCG becomes incomplete for brightest galaxy magnitudes fainter than $R = 12.5$, to the point where at $R = 14.44$, the differential completeness falls to roughly 5%. The surface densities of the $mpCGs$ limited to magnitude brighter than $R < 11.6$ (roughly corresponding to $b_J = 13$) are $7.5, 6.6, 11.8 \times 10^{-3} \text{ deg}^{-2}$, for B06, C06 and DLB, respectively, typically 10 times that the surface density of the $pHCGs$. However, once we limit groups to the nearby subsample, the strong incompleteness at faint magnitudes appears barely visible (B06 and C06) or reversed (DLB), as seen in Figure 4.

The incompleteness of the $pHCG$ in dominant brightest galaxy groups had already been noticed by Prandoni et al. (1994), who also found that Hickson (1982) was biased in favour of groups where the two brightest galaxies have comparable magnitudes.

2.10 Mock Hickson compact groups

As noted above, the HCGs produced by Hickson’s visual inspection cannot be reproduced by an automatic searching algorithm given the many biases in the selection of HCGs. Therefore, the nature and properties of the mock CGs that strictly meet the HCG criteria mentioned in Sect. 2.6 may be different from the properties of the HCGs themselves.

Given the strong and progressive incompleteness of the HCGs in brightest galaxy counts, small angular sizes, and systems with strongly dominant brightest galaxies, it is essential to fold in these extra factors of incompleteness when building a sample that will be a good mock for the observed HCGs. We therefore wish to construct a mock velocity-selected Hickson Compact Group (*mvHCG*) sample, starting with the *mvCG* sample, and selecting galaxies with probabilities proportional to the completeness in 1) group surface brightness, 2) brightest galaxy magnitude, and 3) difference between the brightest galaxy and total group magnitude (i.e. the relative importance of the brightest galaxy). We do not consider the distribution of angular sizes, since this latter quantity is directly dependent on the three other parameters.

Because the resulting number of *mvHCGs* turns out to be very small, rather than select *mvCGs* according to the probability that a given *mvCG* would be observed by Hickson, we proceeded as follows. We selected the first *mvCGs* that fill the observed distribution of *vHCGs* for the three parameters and stopped once one of the 10 bins in any of the three distributions for the *mvCGs* reaches the value observed in the corresponding bin for the *vHCGs*. Hence, the derived distributions of the three parameters do not match perfectly the observed ones, but are lower limits. We repeated this exercise, using different orders for our loop over the *mvCGs* until we matched as best as possible the observed *vHCG* distributions. This procedure was again applied on the eight different samples corresponding to the eight observers situated at the eight vertexes of the simulation cube obtaining final samples of typically 250 *mvHCGs*.

The distribution of properties of *mvHCGs*, shown in Figure 5 for the DLB model, matches much better the observed distributions of *vHCGs*. Similar results are found using the other two SAMs. The three SAMs fail to find groups of roughly concordant magnitudes.

The three *mvHCG* samples will be used to compare with the properties of observed *vHCGs* and with the correlations obtained for previous authors based on the observed accordant-velocity HCGs.

3 DIFFERENT CLASSES OF COMPACT GROUPS

Even though we have used redshift information to identify our *mvCGs*, the selected groups are not necessarily physically dense in 3D real space.

Our *mvCGs* can thus be split into three classes:

- Physically dense groups (Real),
- Chance alignments within loose groups (CALG),
- Chance alignments within filaments (CAF).

Keeping with the original intent of Hickson (1982), who had

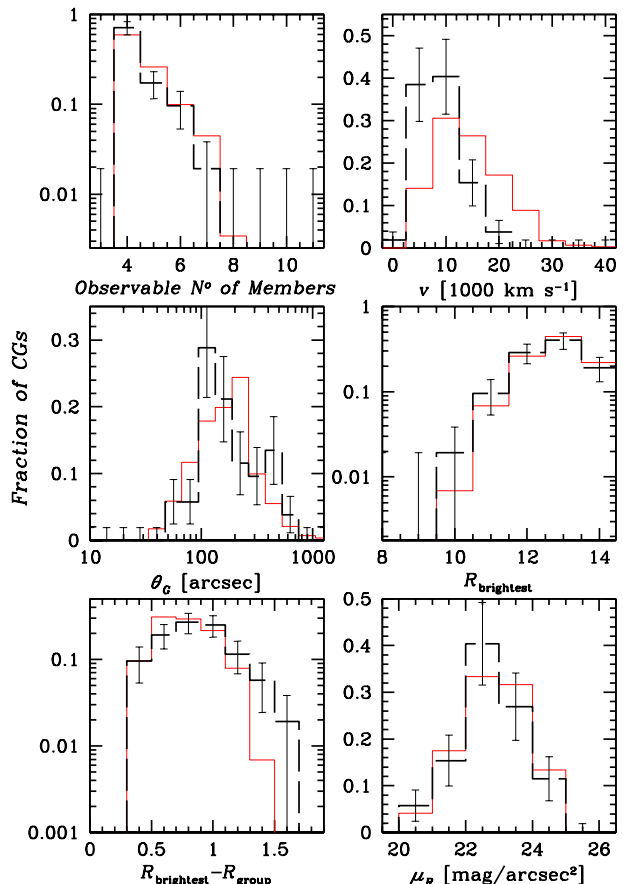


Figure 5. Same as Figure 2 for the *mvHCGs* from the De Lucia & Blaizot SAM (*thin red histograms*) and (again) the observed *vHCGs* (*thick black dashed histograms*).

selected in projection compact groups of at least four galaxies, we will classify an *mvCG* as Real if at least 4 of its galaxies form a physically dense group. Also, we will sometimes join the CALG and CAF classes into the set of Chance Alignments (CAs).

There are several ways to use the three-dimensional information to define these classes, and as we shall see, none of them are perfect.

3.1 Binding energies

A simple way to separate the Real CGs from the CAs is to use the binding energy of the system. In appendix B, we show that binding energies are highly inaccurate for groups of masses $M < 10^{14} h^{-1} M_{\odot}$, and cannot be used to distinguish which CGs are physically dense and which are caused by chance alignments.

3.2 Line-of-sight shape and 3D length

Alternatively, we can classify the mock CGs using their size and/or elongation. We consider the 4 closest galaxies in each mock CG, again in line with the original intent of Hickson (1982). By closest 4 galaxies, we mean either the entire

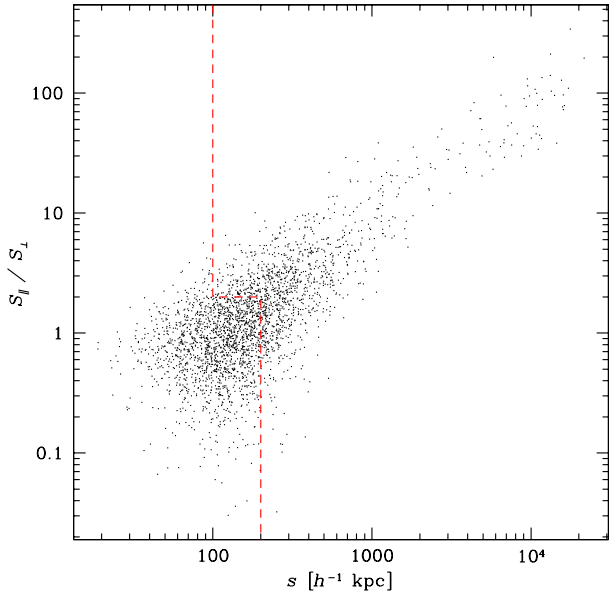


Figure 6. Line-of-sight elongation vs. maximum 3D separation of mock velocity-filtered compact groups extracted from the De Lucia & Blaizot (2007) model. The red dashes delimit the Real *mvCGs* with the hybrid classification discussed below.

mvCG if it has only 4 galaxies, or else the subgroup of 4 with the smallest 3D length. We use the following notations for these smallest quartets:

- s : maximum 3D separation, hereafter *3D length*;
- S_{\perp} : maximum projected separation, hereafter *projected size*;
- S_{\parallel} : maximum line-of-sight separation, hereafter *line-of-sight length*;
- S_{\parallel}/S_{\perp} : hereafter, *line-of-sight elongation*;
- *round mvCG*: $S_{\parallel}/S_{\perp} < 2$;
- *elongated mvCG*: $S_{\parallel}/S_{\perp} \geq 2$.

Figure 6 shows how the line-of-sight elongation is related to the maximum 3D separation. The points in the lower left part of Figure 6 show uncorrelated line-of-sight elongation and 3D length, as expected for Real groups, while the upper right part of the figure shows instead a strong correlation of line-of-sight elongation with 3D length, indicative of CA groups. Which cuts in line-of-sight elongation and 3D length separate best the Real CGs from the CAs? The choice of the critical 3D length, s_{cut} , is not straightforward, as we shall now discuss.

3.2.1 Matching line-of-sight elongation of real-space selected groups

We first tried varying s_{cut} by imposing that the median line-of-sight elongation be equal to that of real-space-selected groups. We measured a median line-of-sight elongation of 0.725 for the PG3Ds. We also checked this median value of the line-of-sight elongation with Monte-Carlo simulations of quartets distributed at random in a virial sphere with an NFW density profile with concentration $r_v/r_s = 10$, where we then elongated the sphere in two orthogonal directions

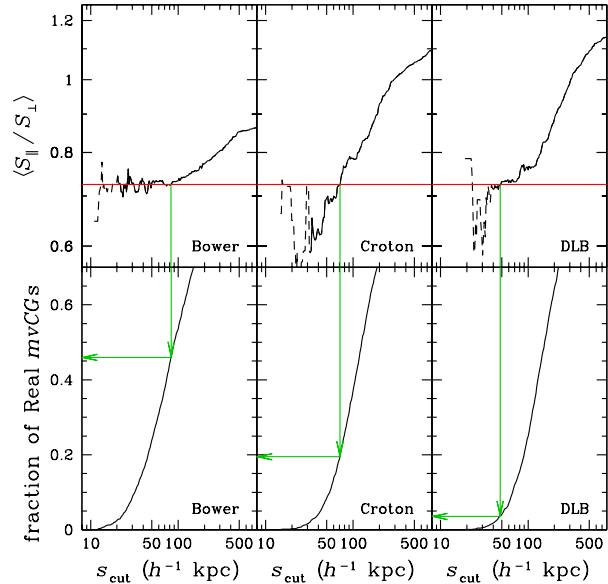


Figure 7. *Upper panels:* Median line-of-sight elongation vs. critical 3D length, s_{cut} , for the 4 galaxies in the richest subclump of mock velocity-accordant compact groups. *Dashed (solid) lines* refer to values of s_{cut} where the sample of *mvCGs* has less (more) than 50 *mvCGs*. The red solid horizontal lines correspond to the median line-of-sight elongation measured by selecting 4 galaxies at random from each *PG3D* group. *Lower panels:* Normalised cumulative distribution of 3D lengths, considered as critical separations between the Real and CA classes. The green arrows indicate the value of s_{cut} that matches the median line-of-sight elongations of the *PG3D* groups (vertical arrows) yielding the corresponding fraction of Real CGs for the adopted s_{cut} (horizontal arrows).

by two factors to make it a triaxial ellipsoid, and observed it from a random direction, and repeated this exercise 5000 times. We then find median line-of-sight elongations of 0.782 (in spheres) and 0.719 (in triaxial ellipsoids, with $b/a = 0.79$ and $c/a = 0.65$, as found by Jing & Suto (2002), on average, in Λ CDM halos at overdensity 100). This median line-of-sight elongation for triaxial halos is very close to what we measured for the PG3Ds.

We also considered the cores of virialized groups, where the overdensity is 10^5 , close to how overdense HCGs appear to be. Here we, limited the particles to a radius of 0.025 virial radii, i.e. 0.25 scale radii (with our concentration of 10), where the mean density is roughly 1000 times greater than at the virial radius. Noting that Λ CDM halos are less spherical at overdensities as high as 10^5 (Jing & Suto find $b/a = 0.61$ and $c/a = 0.46$, on average), we consider these less spherical halos and then find a median line-of-sight elongation of 0.722 (even closer to the median elongation of the PG3Ds). In general, the median line-of-sight elongation is much more sensitive to the triaxiality of the object than to the slope of its density profile.

As seen in the top panels of Figure 7, the values of s_{cut} required for the shortest *mvCG* to reproduce the median line-of-sight elongation of the real-space selected PG3Ds are fairly small and vary from SAM to SAM, from $\sim 50 h^{-1}$ kpc for DLB to $\sim 80 h^{-1}$ kpc for B06, with C06 in between. The bottom panels of Figure 7 indicate that the fraction of

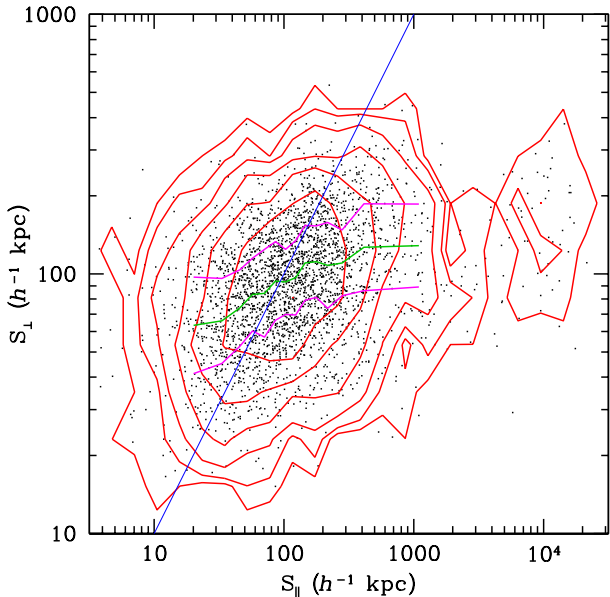


Figure 8. Projected size versus line-of-sight length for the smallest quartets within *mvCGs*, using the De Lucia & Blaizot (2007) SAM. Also shown are log-spaced contours (red), the medians in bins of 200 points (green jagged line) the interquartiles (magenta jagged lines), and the line $y = x$ (thin blue line).

mvCGs whose 3D length of their smallest subclump of four galaxies is less than the corresponding s_{cut} varies strongly with the SAM: 40% with B06, 20% with C06, but only 4% with DLB. This should not lead us to conclude that most *mvCGs* are CAs, because the minimum 3D length (s_{cut}) for CAs with the DLB model is only half the median projected size of the DLB *mvCGs*, which does not seem reasonable. In other words, it is not reasonable to force redshift-space selected groups to be as round as real-space selected ones: redshift-space selection will always produce somewhat more elongated groups than real-space selected ones.

3.2.2 Line-of-sight elongation versus line-of-sight size

Alternatively, one could argue that CAs should be long in the absolute, i.e. high s , and/or relative to their projected sizes, i.e. high S_{\parallel}/S_{\perp} , e.g. $S_{\parallel}/S_{\perp} > 2$.

If the projected sizes were independent of the line-of-sight lengths, as would be expected if all CGs were CAs, we could then impose a value of s_{cut} that would be close to $\sqrt{2}$ times the upper envelope of the S_{\perp} (since round CGs would have $s \simeq \sqrt{S_{\perp}^2 + S_{\parallel}^2} \simeq \sqrt{2} S_{\perp}$).

Figure 8 shows that the *mvCGs* behave differently: while at high line-of-sight length, where CAs are expected to be dominant, the projected size is indeed independent of the line-of-sight length, at low line-of-sight length, where CAs are not dominant, the projected size increases with increasing line-of-sight length. So the upper envelope of the projected sizes is not a clear-cut value. The contours suggest a close to linear increase of S_{\perp} with S_{\parallel} in the low S_{\parallel} regime, as expected for systems of same line-of-sight elongations and different sizes.

The transition between these two regimes is difficult to ascertain. One way is to look for the value of S_{\parallel} for which the median S_{\perp} changes from a high to low slope. This yields a critical S_{\parallel} of $\approx 140 h^{-1}$ kpc for the DLB model (see Fig. 8), $120 h^{-1}$ kpc for the B06 model and $165 h^{-1}$ kpc for the C06 model. These 3 critical values of S_{\parallel} correspond to $S_{\perp} \simeq 100, 105$ and $112 h^{-1}$ kpc, for the B06, C06 and DLB models, respectively. One therefore infers critical group length of $s_{\text{cut}} = 156, 196$ and $179 h^{-1}$ kpc, for the B06, C06 and DLB models, respectively.

The fraction of *mvCGs* with lengths smaller than these three values of s_{cut} can then be read from the bottom panel of Figure 9: one finds 72%, 72% and 59% of the groups have $s < s_{\text{cut}}$ for the B06, C06 and DLB models, respectively. One would therefore deduce that between half and three-quarters of the *mvCGs* are Real (depending on the SAM). However, given the crudeness of the method, one should take these percentages with caution.

3.2.3 Reasonable cuts in length and line-of-sight elongation

We now explore whether reasonable limits on s_{cut} and S_{\parallel}/S_{\perp} can reduce substantially the fraction of Real *mvCGs*. Figure 9 displays the distributions of the 3D length, s , for the DLB model.

The distribution of 3D lengths clearly shows a dominant log-normal component and a second component of more extended lengths. In fact, when restricting to round groups ($S_{\parallel}/S_{\perp} < 2$), the distributions of 3D lengths appear very close to lognormal. Moreover, the round *mvCGs* tend to be smaller with the Bower model ($\langle s \rangle = 78 h^{-1}$ kpc) and larger with the DLB model ($\langle s \rangle = 125 h^{-1}$ kpc), with the predictions from the Croton model in between. Finally, the distribution of elongated *mvCGs* ($S_{\parallel}/S_{\perp} \geq 2$) is wider than that of the round *mvCGs*, and centred around $s \simeq 250 h^{-1}$ kpc for the B06 and C06 models and $300 h^{-1}$ kpc for the DLB model. It displays an extended tail of very large ($> 2 h^{-1}$ Mpc) 3D lengths.

The discussion above suggests a conservative maximum for the Real *mvCGs* of $s_{\text{cut}} < 200 h^{-1}$ kpc.

3.3 Fraction of CAs in different samples of mock CGs

Table 5 summarises the fractions of CGs satisfying various criteria that could classify them as Real. With our choice of $s_{\text{cut}} = 200 h^{-1}$ kpc, we obtain fractions of Real *mvCGs* of 0.80 (Bower), 0.73 (Croton) and 0.64 (DLB). To be more favourable to the CAs, we can include additional elongated *mvCGs*. However, it makes no sense to call a CA an elongated *mvCG* with a very small 3D length, for example with $s = 50 h^{-1}$ kpc, because such an *mvCG* is also a physically dense group, hence a Real. So, we consider a simple hybrid classification (dashed lines in Fig. 6), where the CAs are the *mvCGs* with $s \geq 200 h^{-1}$ kpc OR ($s > 100 h^{-1}$ kpc AND $S_{\parallel}/S_{\perp} \geq 2$). We then find (Table 5) that the fraction of Real *mvCGs* is 0.76 (Bower), 0.67 (Croton), and 0.59 (DLB). We hereafter adopt this hybrid criterion to estimate the fraction of Real and CA compact groups.

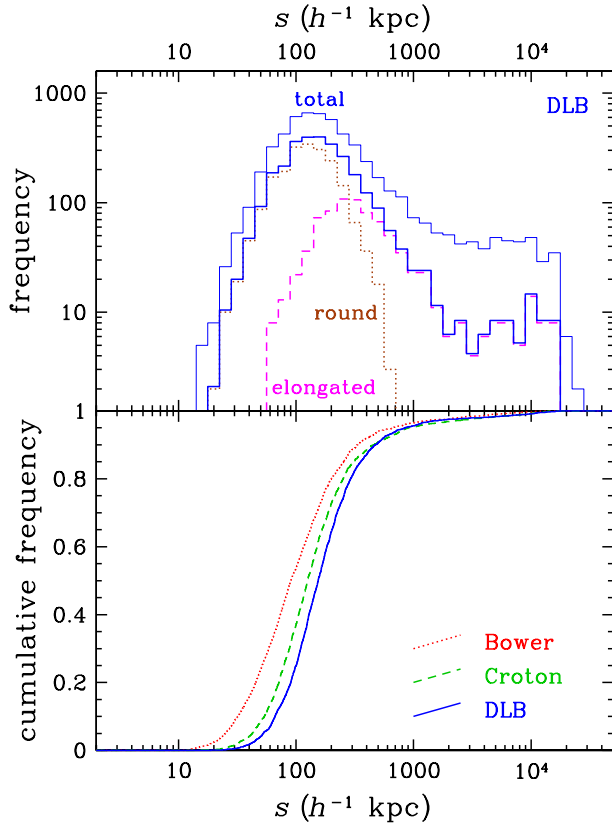


Figure 9. *Top:* Distribution of 3D lengths for the DLB model for all *mvCGs* (solid histograms pushed up by 20% for clarity), the round *mvCGs* ($S_{\parallel}/S_{\perp} < 2$, dashed histograms), and the elongated *mvCGs* ($S_{\parallel}/S_{\perp} \geq 2$, dotted histograms). The thin solid blue curve shows the total distribution for the *pmvCGs*. *Bottom:* Cumulative distribution of 3D lengths of all *mvCGs*.

It therefore, appears that *more than half of the mvCGs are physically dense*, although there are important variations between the three galaxy formation models, with Bower et al. predicting the most physically dense *mvCGs*, De Lucia & Blaizot predicting the least, and Croton et al. in between.

If we only consider CGs identified in projection (*mpCGs*), the Real CGs represent between 35% and 47%, depending on the criteria and on the SAM (Table 5).

We note that the fraction of CAs diminishes in all three SAMs when going from the *pmvCG* to *mvCG* and to *mvHCG* samples, i.e. when first taking into account the extended nature of galaxies causing confusion, and then in incorporating the biases we measured in the visual selection of Hickson (1982). Table 5 thus indicates that the fraction of CAs is 28–47% for the *pmvCGs*, but is reduced to 24–41% for the *mvCGs* and only 14–30% for the *mvHCGs*.

3.4 Chance alignments within Loose Groups and beyond

We now consider as CAs all *mvCGs* with 3D lengths $s \geq 200 h^{-1}$ kpc, regardless of the line-of-sight elongation. The distinction between CALG and CAF is very simple, as we

Table 5. Fraction of Real mock CGs using different criteria

Criterion	B06	C06	DLB
<i>pmvCG</i>			
$s < 200 h^{-1}$ kpc	0.46	0.39	0.22
$S_{\parallel}/S_{\perp} < 2$	0.43	0.38	0.23
$s < 100 h^{-1}$ kpc OR ($s < 200 h^{-1}$ kpc AND $S_{\parallel}/S_{\perp} < 2$)	0.43	0.36	0.20
<i>mpCG</i>			
$s < 200 h^{-1}$ kpc	0.46	0.47	0.38
$S_{\parallel}/S_{\perp} < 2$	0.46	0.46	0.43
$s < 100 h^{-1}$ kpc OR ($s < 200 h^{-1}$ kpc AND $S_{\parallel}/S_{\perp} < 2$)	0.44	0.43	0.35
<i>pmvCG</i>			
$s < 200 h^{-1}$ kpc	0.77	0.70	0.59
$S_{\parallel}/S_{\perp} < 2$	0.71	0.68	0.61
$s < 100 h^{-1}$ kpc OR ($s < 200 h^{-1}$ kpc AND $S_{\parallel}/S_{\perp} < 2$)	0.72	0.64	0.53
<i>mvCG</i>			
$s < 200 h^{-1}$ kpc	0.80	0.73	0.64
$S_{\parallel}/S_{\perp} < 2$	0.80	0.72	0.71
$s < 100 h^{-1}$ kpc OR ($s < 200 h^{-1}$ kpc AND $S_{\parallel}/S_{\perp} < 2$)	0.76	0.67	0.59
<i>mvHCG</i>			
$s < 200 h^{-1}$ kpc	0.91	0.83	0.76
$S_{\parallel}/S_{\perp} < 2$	0.84	0.73	0.76
$s < 100 h^{-1}$ kpc OR ($s < 200 h^{-1}$ kpc AND $S_{\parallel}/S_{\perp} < 2$)	0.86	0.75	0.70

Table 6. Fraction of chance alignments that extend beyond their parent loose group (CAFs)

Sample	B06	C06	DLB
<i>pmvCG</i>	0.32	0.30	0.30
<i>mvCG</i>	0.24	0.24	0.17
<i>mvHCG</i>	0.16	0.26	0.26

simply check whether all CALG members lie within a single PG3D (making it a CALG) or not (making it a CAF).

Table 6 shows that large majority of the CAs (typically three-quarters) are CALGs, regardless of the SAM and the sample. Thus, alignments within filaments or with galaxies in the field are much less likely than chance alignments within larger groups or than having physically dense groups.

3.5 Isolated dense groups?

The standard picture is that dense groups of galaxies are the cores of virialized looser groups. However, some HCGs appear extremely isolated (Rood & Williams 1989; Palumbo et al. 1995). The simulations that we have analysed allow us to check whether dense groups can be isolated out to the virial radius. We have simply cross-identified the *mvCGs* with the real-space-selected PG3Ds. We then call a CG isolated if it constitutes the entire PG3D (in the magnitude range determined by the brightest galaxy of the CG). We then find that only $\sim 11\%$ of the *mvCGs* constitute the entire PG3D in all the three SAMs. In the *mvHCG* samples, the fraction of isolated CGs are somewhat smaller (7% for B06, 6% for C06, and 8% for DLB).

4 DISCUSSION AND CONCLUSIONS

4.1 Summary of results

The aim of this paper is twofold: 1) predicting the nature of automatically identified CGs, and 2) predicting the nature of the well-studied but highly incomplete and biased HCGs. We identify CGs in three mock galaxy catalogues, constructed from the Millennium Simulation at $z = 0$ combined with three semi-analytical models (Bower et al. 2006; Croton et al. 2006; De Lucia & Blaizot 2007). Several thousand mock CGs are identified using a two dimensional automated algorithm similar to that applied by Hickson (1982) plus a restriction in the brightest galaxy magnitude. We also allowed for CGs that contain isolated and compact subgroups and furthermore considered the important effects of extended galaxies causing confusion for close projected pairs.

Our main results are:

(i) Among the observable *mpCGs*, $\sim 60\%$ have at least 4 galaxies within 1000 km s^{-1} of the median velocity of the group, regardless of the SAM. Since our study is carried out on a sample with a redshift cut-off ($z \sim 0.17$), we tested whether our results might be bias by this fact. We find that identifying in our (magnitude+)volume limited catalogue produces 1.6 times more *mvCGs* than identifying on an only-magnitude limited catalogue, because our box sample misses distant galaxies that spoil the isolation of mock Compact groups. Correcting for this effect, we deduce that the fraction of *mpCGs* that survive the velocity filter is 50%. In comparison, there are as many as 52 *vHCGs* among 72 *pHCGs*, meaning that 71% of observed HCGs survive the velocity filter. Given binomial statistics the probability that we find as many as 52 given that 36 (half of 72) are expected is negligible ($P = 0.0\%$).

(ii) Comparing the space densities of the *mvCGs* and the *vHCGs*, we deduce that the HCG catalogue is only 8% complete. A comparison of the parameter distributions between the *mvCGs* and *vHCGs* indicates that the HCG is incomplete in groups of small angular sizes, high fraction of light in the brightest galaxy, as well as (for the C06 model) faint brightest galaxy magnitudes and low surface brightness.

(iii) We find that the velocity filtering of *mpCGs* does not necessarily imply that the resulting accordant-velocity CGs are physically dense. We tested different criteria to classify the accordant-velocity CGs according to the maximum 3D galaxy separations and the line of sight elongations. We find that, with the most conservative criterion, *at least 3/5 of the mock accordant-velocity CGs are physically dense*, although the precise fraction depends on the galaxy formation model used.

(iv) The large majority of non-Real mock accordant-velocity CGs are caused by chance alignments within larger groups, rather than within larger regions such as large-scale filaments.

(v) We find that the fraction of chance alignments decreases from 28–47% for the particle-based *pmvCGs* to 24–41% for the sample with close pairs removed (*mvCGs*) to only 14–30% once we fold in the biases of the HCG (*mvHCGs*). This explains in part why simulation studies (Mamon 1986; Walke & Mamon 1989; Hernquist et al.

1995) predict more chance alignments than one infers from actual observations.

Table 4 indicates that typically half of the groups are lost once we apply the criterion to blend close projected pairs of galaxies. While the discarded groups no longer satisfy the selection threshold of 4 galaxies within 3 magnitudes from the brightest, there are still many blended pairs within the groups that survived the blending criterion (in 1/3, 1/4, and 1/8 of the mock CGs for B06, DLB, and C06, respectively, with similar fractions for *mpCGs* and *mvCGs*). Could this mean that a significant fraction of the *pHCGs* and *vHCGs* contain blended galaxies?

A comparison of the lists of Hickson (1982) (selected from photographic plates) and Hickson et al. (1989) (CCD-based) indicates that the latter found 10 HCGs with extra galaxies (24, 26 [+3], 27, 43, 51, 70, 72, 76[+2], 83 and 99), plus one with one galaxy less (HCG 40). So 10% of the original HCG groups contained blended galaxies as discovered with the better CCD photometry. It therefore appears that our fractions of 1/8 to 1/3 of *mpCGs* with blended pairs is high. But if the truth is in between our particle case and our extended case, then we should have of order 6–17% of groups with blended galaxies, which is in rough agreement with what we see in the HCGs.

Now, three HCGs have been observed at much higher resolution with HST imaging. One shows no extra galaxies (HCG 87), while the other two show more interacting units than counted by Hickson et al. (1989): HCG 31 seems to have 7 galaxies and not just 4, while HCG 90 has 5 galaxies and not 4. Binomial statistics suggest that, with 95% confidence, the view of 2 groups out of 3 with extra galaxies implies that the fraction of such groups with blended pairs is between 14% and 86%. But HST is probably biased towards dense interacting HCGs. Still, there could be interacting pairs showing galaxies that have been blended even with the CCD images of Hickson et al. (1989). So, with the high resolution of the HST, the fraction of *pHCGs* and *vHCGs* with blended pairs may be considerably higher than 10% and in agreement with the fractions found in the mock CGs.

We can also estimate the number of HCGs that are physically dense groups of at least 4 galaxies. As discussed in Sect. 2.1, the HCG catalogue has 100 members, among which 99 are compact groups (since HCG 54 is a collection of H II regions), of which only 83 actually fulfil the original magnitude concordance criterion (*R*-band magnitude range less than 3). Among the 72 *pHCGs* whose brightest and faintest galaxies are brighter than $R = 14.44$ and $R = 17.44$, respectively, only 52 (72%) have at least 4 accordant velocities, and among these, we expect roughly between 36 and 44 HCGs that are physically dense groups of at least 4 galaxies. Extrapolating to the 68 accordant-velocity HCGs (including those with magnitude range greater than 3 mags), *we expect no more than ~ 58 physically dense HCGs with at least 4 galaxies.*

In comparison, Mamon (1986) had predicted that 47 out of what he thought would be 78 accordant velocity HCGs are caused by chance alignments (60%), while the remaining 40% are physically dense (but he predicted that half of these dense groups were unbound systems). We are therefore less pessimistic than Mamon (1986) on the fraction

of chance alignments polluting the HCG catalogue, since chance alignments appear to represent between 14% and 30% of the *mvHCGs* (we were not able to check what fraction of the Real ones are unbound: see Appendix B). Part of this discrepancy is caused by Mamon’s (1986) reliance on simulations without consideration of selection effects such as observers blending close projected pairs of galaxies. Still, the percentage of chance alignments in the particle mock velocity-filtered compact groups (*pmvCGs*) is only 28–47% (depending on the SAM). Nevertheless, given the wide range of chance alignments fractions among the three SAMs, one cannot rule out that a more realistic galaxy formation model would lead to as much as 60% of chance alignments.

4.2 Comparison with McConnachie et al.

McConnachie et al. (2008) (MEP) have published a study very similar to ours: they also extracted *pmvCGs* from the DLB model obtained from the Millennium dark matter simulations. Their sample extended to $r = 18$, which corresponds to roughly one-quarter of a magnitude fainter than our limit of $R < 17.44$. Their other *pmvCG* criteria appear to be almost exactly the same as ours (following the criteria of Hickson 1982), although their algorithm works differently (McConnachie et al. 2009). MEP found a total of over 15 000 *pmvCGs* over 4π sr.

Using precisely the same input galaxy catalogue (from Blaizot et al. 2005) as MEP, we find 25 000 *pmvCGs*, so, our algorithm is nearly 1.6 times more efficient than MEP’s in finding *pmvCGs*. Surprisingly, if we build a light cone as we did in Sect. 2.8, with apparent magnitude limit of $R = 17.67$ ($\simeq r_{\text{SDSS}} = 18$), we obtain a mock galaxy catalogue that is 3 times denser than the Blaizot et al. mock galaxy catalogue used by MEP. From our mock galaxy catalogue, we extract 15 191 *pmvCGs* in 1.2693 sr, which means that, with the data used in this work, we are ~ 10 times more efficient than MEP in finding CGs, principally by differences in the parent samples of galaxies, but also by differences in the CG detection algorithm.

MEP and us agree that a significant fraction of *mpCGs* are caused by chance alignments: MEP found 71% of their *mpCGs* are CAs while we find 80% (with our hybrid classification, see Table 5).

There are, however, several important differences between our two studies:

- MEP build their sample from a mock that extends beyond the box size of the Millennium simulation — using the output of the Mock Map Facility (MoMaF) code of Blaizot et al. (2005), while our mock galaxy catalogues are limited to the size of the simulation box. However, as shown in Sect. 2.8, working on a light cone or working on a single simulation box leads to similar numbers of mock CGs (we identify a factor of 1.2 fewer *mpCGs*, and 1.5 more *mvCGs*).

- MEP consider CGs with a faint magnitude limit, while we also tie in a bright magnitude limit to ensure that all mock CGs were built from galaxies that spanned a range of over 3 magnitudes.

- We have analysed the galaxies from 3 different SAMs, while MEP have only considered the DLB sample, which we found to produce the smallest fraction of physically dense *mpCGs*.

- MEP only provide statistics for the mock CGs defined in projection (*pmvCGs*, which they refer to as ‘HA’s’) but do not consider the subset of accordant-velocity groups (*pmvCGs*). We think this would have been worthwhile because ever since Hickson et al. (1992) published the HCG galaxy redshifts, most analyses have thrown out the discordant velocity HCGs.

- MEP did not consider selection effects, while we considered both the galaxy confusion from close, blended, projected pairs, as well as the biases that we determined for the Hickson’s visual selection of the HCGs.

- MEP only considered those *mpCGs* with $k \geq 3$ galaxies that lie very close in real space, while we considered $k \geq 4$ (to be consistent with Hickson’s initial motivation to have at least 4 galaxies per HCG).

- MEP define the Real *mpCGs* using a Friends-of-Friends linking length in real space, while we use a maximum real-space separation and the elongation along the line-of-sight. Structures built from small numbers of components with Friends-of-Friends algorithms tend to be more filamentary (e.g. Moore, Frenk, & White 1993). For *mpCGs* that are CALGs or CAFs, the most distant outlier will determine a similar maximum length and critical linking length. However, for *mpCGs* without outliers (e.g. Real *mpCGs*), the linking length will be smaller than the 3D length. In other words, selecting Real groups with a linking length of $200 h^{-1}$ kpc will result in group 3D lengths considerably greater. Moreover, for *mpCGs* with both foreground and background galaxies, MEP’s ℓ must be compared to our *half*-maximum size $s_{\text{cut}}/2$, and there is here a discrepancy of a factor two. Worse, for those (admittedly rare) cases of, say 4, galaxies aligned along the line of sight at roughly equal separations just below ℓ , one will end up with a group that spans up to $3\ell = 600 h^{-1}$ kpc, which is now three times our maximum 3D length, but will still be called *Compact Association* (Real) by MEP, although it clearly is a chance alignment. In summary, this point and the previous one imply that MEP’s criterion for calling an *mpCG* Real is much more liberal than ours.

4.3 Perspectives

In forthcoming papers, we will analyse the distribution of and correlations between the physical characteristics of the *mvCGs*, and show how they depend on their classification, in view of optimising the probability that a CG selected in redshift-space is physically dense. It would be worthwhile to probe the formation of the physically dense CGs by analysing the merger trees of galaxies in the mock CGs. Finally, the analysis presented here will need to be confirmed with increasingly realistic simulations of galaxy catalogues, for example constructed from future galaxy formation models run on the recent high resolution Millennium-II dark matter simulation (Boylan-Kolchin et al. 2009), and also on future high-resolution cosmological hydrodynamical simulations, with realistic prescriptions for feedback from AGN and supernovae.

5 ACKNOWLEDGEMENTS

We thank Paul Hickson, Abilio Mateus and Jack Sulentic for useful exchanges and an anonymous referee for interesting comments. The Millennium Simulation databases used in this paper and the web application providing online access to them were constructed as part of the activities of the German Astrophysical Virtual Observatory. We thank Richard Bower, Darren Croton, and Gabriele De Lucia for allowing public access for the outputs of their very impressive semi-analytical models of galaxy formation. This research has made use of Vizier database maintained by the Center de Données Stellaires in Strasbourg, France, and the NASA/IPAC Extragalactic Database (NED) which is operated by the Jet Propulsion Laboratory, California Institute of Technology, under contract with the National Aeronautics and Space Administration. This work was partially supported by the European Commission's ALFA-II program through its funding of the Latin-American European Network for Astrophysics and Cosmology (LENAC), Consejo de Investigaciones Científicas y Técnicas de la República Argentina (CONICET), the Agencia Nacional de Promoción Científica and the Secretaría de Ciencia y Técnica de la Universidad Nacional de Córdoba (SeCyT).

REFERENCES

- Allam S. S., Tucker D. L., 2000, *Astronomische Nachrichten*, 321, 101
- Arhipova V. P., Afanasev V. L., Dostal V. A., Zasov A. V., Karachentsev I. D., Noskova R. I., Saveleva M. V., 1981, *Soviet Astronomy*, 25, 277
- Barnes J., 1985, *MNRAS*, 215, 517
- Barton E., Geller M., Ramella M., Marzke R. O., da Costa L. N., 1996, *AJ*, 112, 871
- Barton E. J., de Carvalho R. R., Geller M. J., 1998, *AJ*, 116, 1573
- Bertone S., De Lucia G., Thomas P., 2007, *MNRAS*, 379, 1143
- Blaizot J., Wadadekar Y., Guiderdoni B., Colombi S. T., Bertin E., Bouchet F. R., Devriendt J. E. G., Hatton S., 2005, *MNRAS*, 360, 159
- Bode P. W., Cohn H. N., Lugger P. M., 1993, *ApJ*, 416, 17
- Bower R. G., Benson A. J., Malbon R., Helly J. C., Frenk C. S., Baugh C. M., Cole S., Lacey C. G., 2006, *MNRAS*, 370, 645
- Boylan-Kolchin M., Springel V., White S. D. M., Jenkins A., Lemson G., 2009, *MNRAS*, 398, 1150
- Bryan G. L., Norman M. L., 1998, *ApJ*, 495, 80
- Cardelli J. A., Clayton G. C., Mathis J. S., 1989, *ApJ*, 345, 245
- Carnevali P., Cavaliere A., Santangelo P., 1981, *ApJ*, 249, 449
- Cattaneo A., Dekel A., Devriendt J., Guiderdoni B., Blaizot J., 2006, *MNRAS*, 370, 1651
- Chabrier G., 2003, *PASP*, 115, 763
- Croton D. J., Springel V., White S. D. M., De Lucia G., Frenk C. S., Gao L., Jenkins A., Kauffmann G., Navarro J. F., Yoshida N., 2006, *MNRAS*, 365, 11
- Cuesta A. J., Prada F., Klypin A., Moles M., 2008, *MNRAS*, 389, 385
- Davis M., Efstathiou G., Frenk C. S., White S. D. M., 1985, *ApJ*, 292, 371
- de Carvalho R. R., Gonçalves T. S., Iovino A., Kohl-Moreira J. L., Gal R. R., Djorgovski S. G., 2005, *AJ*, 130, 425
- de Carvalho R. R., Ribeiro A. L. B., Capelato H. V., Zepf S. E., 1997, *ApJS*, 110, 1
- De Lucia G., Blaizot J., 2007, *MNRAS*, 375, 2
- de Vaucouleurs G., de Vaucouleurs A., Corwin J. R., Buta R. J., Paturel G., Fouqué P., 1991, *Third Reference Catalogue of Bright Galaxies*. Springer, New York
- Deng X.-F., He J.-Z., Jiang P., He C.-G., Luo C.-H., Wu P., 2007, *Astrophysics*, 50, 18
- Diaferio A., Geller M. J., Ramella M., 1994, *AJ*, 107, 868
- Dos Santos S., Mamon G. A., 1999, *A&A*, 352, 1
- Eke V. R., Baugh C. M., Cole S., Frenk C. S., Navarro J. F., 2006, *MNRAS*, 370, 1147
- Falco E. E., Kurtz M. J., Geller M. J., Huchra J. P., Peters J., Berlind P., Mink D. J., Tokarz S. P., Elwell B., 1999, *PASP*, 111, 438
- Focardi P., Kelm B., 2002, *A&A*, 391, 35
- Fukugita M., Shimasaku K., Ichikawa T., 1995, *PASP*, 107, 945
- Hernquist L., Katz N., Weinberg D. H., 1995, *ApJ*, 442, 57
- Hickson P., 1982, *ApJ*, 255, 382
- , 1993, *Astrophysical Letters Communications*, 29, 1
- Hickson P., Kindl E., Auman J. R., 1989, *ApJS*, 7, 687
- Hickson P., Kindl E., Huchra J. P., 1988, *ApJ*, 331, 64
- Hickson P., Mendes de Oliveira C., Huchra J. P., Palumbo G. G., 1992, *ApJ*, 399, 353
- Hickson P., Ninkov Z., Huchra J., Mamon G., 1984, in *Clusters and Groups of Galaxies*, Mardirossian F., Giuricin G., Mezzetti M., eds., Reidel, Dordrecht, pp. 367–373
- Hickson P., Rood H. J., 1988, *ApJ*, 331, L69
- Iovino A., 2002, *AJ*, 124, 2471
- Iovino A., de Carvalho R., Gal R., Odewahn S., Lopes P., Mahabal A., Djorgovski S., 2003, *AJ*, 125, 1660
- Jiang C. Y., Jing Y. P., Faltenbacher A., Lin W. P., Li C., 2008, *ApJ*, 675, 1095
- Jing Y. P., Suto Y., 2002, *ApJ*, 574, 538
- Kelm B., Focardi P., 2004, *A&A*, 418, 937
- Lee B. C., Allam S. S., Tucker D. L., Annis J., Johnston D. E., Scranton R., Acebo Y., Bahcall N. A., Bartelmann M., Böhringer H., Ellman N., Grebel E. K., Infante L., Loveday J., McKay T. A., Prada F., Schneider D. P., Stoughton C., Szalay A. S., Vogeley M. S., Voges W., Yanny B., 2004, *AJ*, 127, 1811
- Lokas E. L., Mamon G. A., 2001, *MNRAS*, 321, 155
- Mamon G. A., 1986, *ApJ*, 307, 426
- , 1987, *ApJ*, 321, 622
- , 1989, *A&A*, 219, 98
- , 1992, in *Distribution of Matter in the Universe*, Mamon G. A., Gerbal D., eds., DAEC mtg. No. 2, Obs. de Paris, Paris, pp. 51–66, ftp://ftp.iap.fr/pub/from_users/gam/PAPERS/daec92cg.ps.gz
- , 2000, in *IAU Coll. No. 174, Small Galaxy Groups*, Valtonen M. J., Flynn C., eds., Vol. 209, ASP, San Francisco, pp. 217–225, [arXiv:astro-ph/9909019](http://arxiv.org/abs/astro-ph/9909019)
- , 2008, *A&A*, 486, 113
- Mateus A., 2008, *MNRAS*, submitted, [arXiv:astro-ph/0802.2720](http://arxiv.org/abs/astro-ph/0802.2720)
- Mateus A., Jimenez R., Gaztañaga E., 2008, *ApJ*, 684, L61

McConnachie A. W., Ellison S. L., Patton D. R., 2008, MNRAS, 387, 1281
 McConnachie A. W., Patton D. R., Ellison S. L., Simard L., 2009, MNRAS, 395, 255
 Mei S., Blakeslee J. P., Côté P., Tonry J. L., West M. J., Ferrarese L., Jordán A., Peng E. W., Anthony A., Merritt D., 2007, ApJ, 655, 144
 Mendes de Oliveira C., Hickson P., 1991, ApJ, 380, 30
 Mendes de Oliveira C. L., Temporin S., Cypriano E. S., Plana H., Amram P., Sodré L. J., Balkowski C., 2006, AJ, 132, 570
 Moles M., del Olmo A., Perea J., Masegosa J., Marquez I., Costa V., 1994, A&A, 285, 404
 Moore B., Frenk C. S., White S. D. M., 1993, MNRAS, 261, 827
 Ochsenbein F., Bauer P., Marcout J., 2000, A&AS, 143, 23
 Ostriker J. P., Lubin L. M., Hernquist L., 1995, ApJ, 444, L61
 Palumbo G. G. C., Saracco P., Hickson P., Mendes de Oliveira C., 1995, AJ, 109, 1476
 Poggianti B. M., 1997, A&A, 122, 399
 Ponman T. J., Bourner P. D. J., Ebeling H., Böhringer H., 1996, MNRAS, 283, 690
 Prada F., Klypin A. A., Simonneau E., Betancort-Rijo J., Patiri S., Gottlöber S., Sanchez-Conde M. A., 2006, ApJ, 645, 1001
 Prandoni I., Iovino A., MacGillivray H. T., 1994, AJ, 107, 1235
 Ramella M., Diaferio A., Geller M. J., Huchra J. P., 1994, AJ, 107, 1623
 Rood H. J., Williams B. A., 1989, ApJ, 339, 772
 Rose J. A., 1977, ApJ, 211, 311
 Rubin V. C., Hunter D. A., Ford W. Kent J., 1990, ApJ, 365, 86
 Salpeter E. E., 1955, ApJ, 121, 161
 Shen S., Mo H. J., White S. D. M., Blanton M. R., Kauffmann G., Voges W., Brinkmann J., Csabai I., 2003, MNRAS, 343, 978
 Springel V., White S. D. M., Jenkins A., Frenk C. S., Yoshida N., Gao L., Navarro J., Thacker R., Croton D., Helly J., Peacock J. A., Cole S., Thomas P., Couchman H., Evrard A., Colberg J., Pearce F., 2005, Nature, 435, 629
 Stephan M. E., 1877, CR Acad. Sci., 84, 641
 Sulentic J. W., 1987, ApJ, 322, 605
 —, 1997, ApJ, 482, 640
 Tovmassian H., Plionis M., Torres-Papaqui J. P., 2006, A&A, 456, 839
 Tovmassian H. M., Yam O., Tiersch H., 2001, Revista Mexicana de Astronomia y Astrofisica, 37, 173
 Verdes-Montenegro L., Del Olmo A., Iglesias-Páramo J. I., Perea J., Vilchez J. M., Yun M. S., Huchtmeier W. K., 2002, A&A, 396, 815
 Walke D. G., Mamon G. A., 1989, A&A, 225, 291
 Xu G., 1995, ApJS, 98, 355
 Zepf S. E., 1993, ApJ, 407, 448

APPENDIX A: FROM R-SDSS TO R-JOHNSON APPARENT MAGNITUDE LIMIT

According to Table 3 of Fukugita, Shimasaku, & Ichikawa (1995), $r-R$ has typical values of 0.36 (E), 0.31 (S0), 0.33 (Sab), 0.32 (Sbc), 0.30 (Scd), and 0.20 (Im), and we adopt $\langle r-R \rangle = 0.33$. We thus restrict the HCG sample to a total extrapolated R band extinction-corrected magnitude

$$R_T^0 = B_T^0 - (B-R)_{\text{iso}} + (B_T - B_T^0) \left(1 - \frac{A_R/A_V}{A_B/A_V} \right) \quad (\text{A1})$$

$$< 17.44 ,$$

where we adopted $A_B/A_V = 1.33$ and $A_R/A_V = 0.75$ (Cardelli et al. 1989). Equation (A1) assumes no $B-R$ colour gradient in the galaxy.

APPENDIX B: GROUP BINDING ENERGIES

The binding energy of the particles of a mock CG is difficult to determine because it is not clear which particles belong to the CG.

One could alternatively use the galaxies instead of the particles. But most of the mass of a group is thought to lie in between the galaxies, so one must be careful on how the binding energy analysis is performed. We separate the group into the system of galaxies and the remaining intergalactic dark matter. The kinetic energy of the group would then be

$$K = K_g + K_d = \frac{3}{2} (M_g + M_d) \sigma_v^2 , \quad (\text{B1})$$

where M_g and M_d are the masses of the galaxies and of the intergalactic dark matter, respectively, while σ_v is the one-dimensional velocity dispersion assumed to be the same for the intergalactic dark matter and the galaxies, and where we placed ourselves in the group centre-of-mass to get rid of the bulk kinetic energy. The potential energy is more difficult to handle as it is the sum of the potential energies of the galaxy system, the intergalactic dark matter system and the cross-term between galaxies and the intergalactic dark matter. Suppose a group has a factor μ times more intergalactic dark matter than mass in galaxies. From equation (B1), the kinetic energy is then

$$K = (\mu + 1) K_g . \quad (\text{B2})$$

If the galaxies and the dark matter have similar distributions in space (which is not really possible, since by definition the intergalactic dark matter is outside the galaxies), then the total potential energy can be written

$$\begin{aligned}
 W &= W_{g,g} + W_{d,d} + W_{g,d} \\
 &= -\frac{GM_g^2}{r_G} - \frac{GM_d^2}{r_G} - \frac{GM_g M_d}{r_G} \\
 &= (\mu^2 + \mu + 1) W_{g,g} , \quad (\text{B3})
 \end{aligned}$$

where r_G is the gravitational radius, assumed to be the same for the three terms. So, if the group is in virial equilibrium, one has $2K + W = 0$, then according to equations (B2) and (B3), one finds that

$$2(\mu + 1) K_g + (\mu^2 + \mu + 1) W_{g,g} = 0 \quad (\text{B4})$$

Therefore, one finds that

$$-\frac{2K_{g,g}}{W_{g,g}} = \frac{\mu^2 + \mu + 1}{\mu + 1}, \quad (\text{B5})$$

so, if the intergalactic dark matter makes up for say $\mu = 4$ times as much as the galaxy mass, then if the group is in virial equilibrium, equation (B5) leads to $-2K_{g,g}/W_{g,g} = 21/5 = 4.2$. Therefore, *the virial ratio of the galaxies in a group can be far off from unity!* It will depend on the fraction of mass in galaxies (i.e. on $1/(\mu + 1)$, hence on μ). Finally, since the virial ratio of the galaxy system appears to be greater than 2, we would incorrectly conclude that typical groups are unbound!

One way to avoid these problems is to assign to each galaxy the fraction of the total group mass equal to the ratio of its mass divided by the total mass in galaxies for that group. In other words, we are putting the intergalactic dark matter mass in each galaxy in proportion to its mass. This is equivalent to $\mu = 0$, hence to a virial ratio of unity according to equation (B5).

The simulation data that we have at our disposal provides the virial masses of the PG3D groups (dark matter included). If a mock CG is a CA, then we cannot know how much dark matter is assigned to this CA, but only to the PG3D group associated with it. We therefore choose to scale the galaxy masses to the PG3D group mass, i.e.

$$m' = \frac{m}{\sum_{i \in \text{PG3D}} m_i} M_{\text{PG3D}}. \quad (\text{B6})$$

Still, there remains the issue of CG galaxies that do not belong to any PG3D. One possibility is to apply equation (B6) to the CG galaxies that lie within PG3D groups, without scaling the masses of the isolated galaxies. The alternative is to scale by the fraction of mass in the whole simulation box, instead of the PG3D group.

Another issue is that the virial spheres around the galaxies will tend to overlap inside the Real CGs. One therefore needs to soften the galaxy-galaxy potential energy of interaction, for example with the approximation (Mamon 1987):

$$V_{\text{int}}(r_{i,j}) = -\frac{Gm'_i m'_j}{\sqrt{r_{i,j}^2 + r_{i,j,\text{rms}}^2}} \quad (\text{B7})$$

where $r_{i,j,\text{rms}}$ is the root mean squared of the half-mass radii of the pair of galaxies $\{i, j\}$. The virial theorem becomes

$$2K + \sum \mathbf{F} \cdot \mathbf{r} = 0, \quad (\text{B8})$$

where the Clausius virial of a group is

$$\begin{aligned} \sum \mathbf{F} \cdot \mathbf{r} &= \sum_i \mathbf{r}_i \cdot \nabla V_{\text{int}}(r_{i,j}) \\ &= \sum_i r_i \cdot \sum_{j \neq i} \mathbf{r}_{i,j} \frac{Gm'_i m'_j}{(r_{i,j}^2 + r_{i,j,\text{rms}}^2)^{3/2}} \\ &= G \sum_{i < j} m'_i m'_j \frac{r_{i,j}^2}{(r_{i,j}^2 + r_{i,j,\text{rms}}^2)^{3/2}} \end{aligned} \quad (\text{B9})$$

where $\mathbf{r}_{i,j}$ is the vector separating galaxies i and j .

But how do we estimate the galaxy half-mass radii? We can compute analytically the half-mass radius of the matter within the virial radius, say for an NFW model, with a concentration $c = r_v/r_{-2} = 10$ (where r_{-2} is the ‘scale’ radius of slope -2), for which $r_h/r_v \simeq 0.36$ (Lokas & Mamon

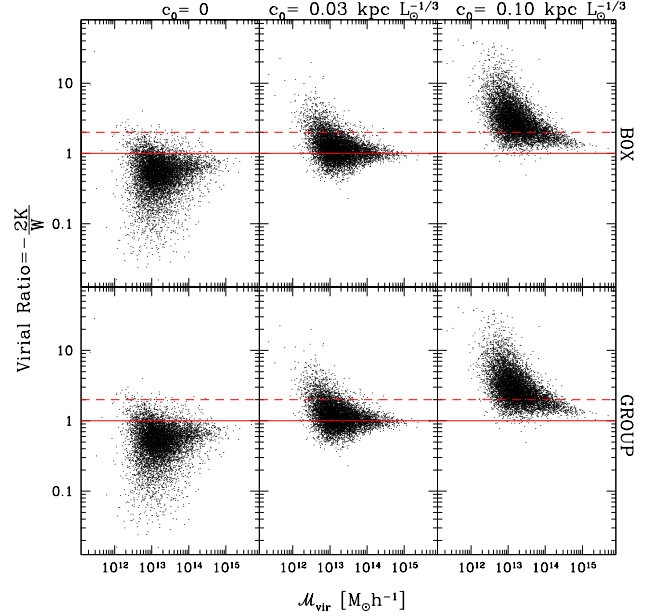


Figure B1. Virial ratio as a function of virial mass for PG3D groups with $N > 10$ members extracted from DLB model, where the galaxy mass correction (eq. [B6]) is over the entire box (*top panel*) or the parent group (*bottom panel*). The *solid red line* shows the expected virial ratio of unity, while the *dashed line* shows the limit for unbound groups.

2001, Fig. 4 and eq. [28]). But we could also compute the half-mass radius within a larger radius, say the turnaround radius beyond which the Universe is expanding, and which is typically 3.5 times the virial radius. Assuming that the NFW model extends that far (see Prada et al. 2006), going to the turnaround radius amounts to increasing the concentration by a factor of $r_{\text{ta}}/r_v \approx 3.5$. So, if $c = 10$ for a galaxy, at the turnaround radius, we would use $c = 35$ and find $r_h/r_{\text{ta}} \simeq 0.23$, i.e. $r_h/r_v \simeq 0.79$.

But then, how do we estimate the mass within the virial radius of the galaxy? We could guess a mass-to-light ratio $M(r_v)/L_B = 100$, although $M(r_v)/L_B$ is thought to decrease with increasing luminosity to reach a minimum around 70 (Eke et al. 2006). Then $r_v = [2/\Delta (GM/H_0^2)]^{1/3} = [2/\Delta (G(M/L)L/H_0^2)]^{1/3} = 544 (L/10^{11})^{1/3} \text{ kpc}$ for $\Delta = 100$ (as we used in the paper), $H_0 = 73 \text{ km s}^{-1} \text{ Mpc}^{-1}$ (as used in the Millennium Simulation) and $M/L = 100$. For $L_* = 0.18 \times 10^{11} L_\odot$, we end up with $r_v = 307 \text{ kpc}$. So for L_* galaxies, we need a softening of typically $r_0 = 70$ to 250 kpc , i.e. $c_0 = r_0/L^{1/3} = 0.03$ to 0.10 . Of course, the higher the softening scale, the less negative is the potential energy and the less bound is the system.

We test our prescription by computing the virial ratios of the PG3Ds using both PG3D scaling and box scaling of the galaxy masses, with different values for the softening scale c_0 . The correct scaling must lead to virial ratios of unity, independent of group mass.

Figure B1 shows the results of our test on PG3D groups. For both normalisations, we find that the softening $c_0 = 0.03 \text{ kpc } L_\odot^{-1/3}$ (corresponding to $r_0 = 70 h^{-1} \text{ kpc}$ for $L = L_*$ galaxies) bring the virial ratios of the highest mass PG3Ds

to unity. Without the softening, the potential energies are overestimated (in absolute value), hence the virial ratios are underestimated, while with too strong softening the virial ratios are overestimated.

However, Figure B1 indicates that even with the correct softening, i.e. with correct virial ratios at the high mass end, there is so much scatter in the virial ratios at low masses, that over 13% of the PG3Ds are found to be unbound for PG3D virial masses below $4 \times 10^{13} M_{\odot}$. This means that for the typical masses of the CGs, our virial ratio estimator is too inaccurate to use as a CG classifier.